Abstract

Wildland firefighters play a critical role in managing the complex relationship between humans and fire. To reduce the inherent risks that come with this role, firefighters use safety protocols such as lookouts, communications, escape routes, and safety zones (LCES). Currently, LCES implementation is conducted on the ground with limited support from geospatial information, despite the protocol's inherently spatial nature. This study introduces GeoLCES: an analytical framework designed to enhance LCES implementation using remote sensing and geospatial modeling. GeoLCES comprises three spatially explicit safety metrics, derived from airborne lidar data: (1) visibility index (VI), which quantifies landscape-wide visibility, aiding the evaluation of lookouts and communications; (2) escape route index (ERI), which quantifies mobility, facilitating the identification of escape routes and avoidance of entrapment-prone area; and (3) proportional safe separation distance (pSSD), which quantifies the relative degree of sufficient fuel separation, enabling the identification of suitable safety zones. In this study, we describe the theory, computation, application, and interpretation of each of these three metrics as a multivariate, pre-fire decision support tool. To highlight implementation on a useful scale, we map GeoLCES at 30m resolution throughout Gila National Forest in New Mexico, USA. We provide an operationally relevant use-case demonstration to exemplify one approach for employing GeoLCES at the incident level. GeoLCES is the first geospatial analytical framework that seeks to specifically address the complex, multivariate nature of LCES in a holistic manner, and has the potential to improve wildland firefighter safety at a time of increasing fire management demands.

Keywords

Wildland fire; decision support; firefighter safety; lidar; LCES; evacuation; visibility; safe separation distance; Gila National Forest

1. Introduction

In an era of increasing wildfire and fire impacts in many regions, it is imperative to develop robust solutions for ensuring the safety of wildland firefighters [1]. Firefighters play a critical role in mitigating loss of life and property by suppressing the dangerous spread of wildfires [2]. They do so in a variety of ways, including the strategic, mechanical manipulation of fuel loads, construction of containment lines, setting backfires to reduce fuels ahead of an advancing fire, and minimizing fuel and infrastructure flammability with water [3]. They are also responsible for conducting prescribed fires, applying fire to the landscape in a more controlled and ecologically-focused manner to prevent the hazardous buildup of fuels. All of these activities are essential for adapting to a more fire-prone present and future, and creating a more sustainable coexistence between humans and fire, particularly in wildland-urban interface settings [4,5]. Unfortunately, in the course of engaging in this life-saving work, firefighters are necessarily placed in hazardous environments and situations. They work long hours, over extended periods, in hot, smoky, and sometimes rugged settings, often in close proximity to flames [6]. As a result, injuries or fatalities can and do occur every year among wildland firefighters in the US and beyond [7].

Firefighters have many tools at their disposal to minimize risks to their health and wellbeing. Among these, operational safety protocols like lookouts, communications, escape routes, and safety zones (LCES) play a particularly important role in keeping firefighters safe [8]. LCES is a system of four interdependent safety measures that, if properly implemented, can minimize the likelihood of injury or fatality. Lookouts are members of a crew strategically positioned on the landscape to maintain an active view of the fire and alert the other members of their crew about changes in weather or fire behavior. Communications are used to relay critical information among a crew, between crews, with incident command, and other relevant entities on a fire incident. Escape routes are efficient ground pathways that firefighters can use to evacuate their position on the landscape in dangerous situations. Safety zones are large, open areas low in fuel that can serve as evacuation destinations, within which firefighters should be safe from nearby or surrounding fire.

Evaluating and implementing LCES on the ground can be a challenging process. For example, on a fire incident that spans hundreds or thousands of hectares, it might be difficult to identify a suitable location to place a lookout that would enable broad-scale visibility of the landscape and fire based on ground-level information alone [9]. Firefighters may struggle to reliably and consistently evaluate how large their safety zone needs to be, given the complexity of visually approximating the safe separation distance needed to avoid burn injury [10,11]. Relying solely on firefighters' perceptions, knowledge, and experience to make these critical safety evaluations on the ground, in real time, may introduce uncertainty into the LCES process.

Many of the landscape conditions that drive LCES effectiveness are inherently spatial, and can be readily mapped using modern geospatial technology. Airborne lidar data in particular offer a valuable solution for accurate, precise, and spatially explicit quantification of landscape characteristics that promote or inhibit firefighter safety [12]. Laser pulses emitted from a sensor mounted on an aircraft towards the ground surface in rapid succession reflect off of the ground, vegetation, or artificial surfaces back to the sensor, yielding a detailed three-dimensional point cloud from which fuel and terrain structure can be mapped [13]. Lidar has shown great promise towards supporting the LCES process, including previous demonstrations of lidar-based metrics for quantifying spatial variation in LCES components [9,11,12,14].

Lookouts benefit from a high degree of landscape visibility. An ideal lookout location would be one where no obstructions are present, enabling direct lines of sight with the fire, crew, and other resources [15]. Communications – especially radio communications – also benefit from high visibility, avoiding signal loss driven by terrain and vegetative barriers [16,17]. Lidar has an unparalleled ability to generate high-resolution digital surface models that incorporate both the terrain and aboveground features (e.g., trees) that promote or hinder visibility, quantifiable with viewshed analysis [18]. Escape routes benefit from landscape conditions that promote efficient foot travel, enabling firefighters to quickly and safely move during an evacuation [19–21]. Lidar is an ideal source of data for quantifying pedestrian mobility, not only being able to precisely map terrain slope, but also characterize fine-scale ground surface roughness and the density of low-lying vegetation, all of which can act to substantially impede movement [12]. Safety zone size and effectiveness are primarily dictated by safe separation distance (SSD): the distance one must maintain from fire (or fuel anticipated to burn) to avoid burn injury [22,23]. SSD is driven by the transfer of radiant and convective heat over space, which can be approximated using vegetation height, terrain slope, wind speed, and burning condition, the first two of which lidar can map with high accuracy [24–26].

Evaluating the individual elements of LCES in isolation, as existing lidar-focused firefighter safety research has done, neglects the critical interdependency of the LCES protocol. For example, even the fastest escape route is useless if it is not connected to a safety zone, and even the best lookout location provides no real value if it cannot be accessed. Furthermore, it is difficult to ask firefighters, whose time and resources are already stretched thin, to separately consider a host of individual firefighter safety spatial products. Thus, for the mutual benefit of conceptual usefulness and operational feasibility, there remains a need for a singular, multivariate approach that simultaneously considers the interconnected nature of LCES in a geospatial context.

In this study, we introduce GeoLCES: a holistic, lidar-driven analytical framework that seeks to improve the efficiency, consistency, and reliability of evaluating and implementing LCES. Our objectives are to describe the conceptual underpinnings and geospatial formulation of GeoLCES' three metrics, apply the GeoLCES framework within a US National Forest to exemplify its operational utility at scale, interpret results in the context of their implications for wildland firefighter safety, and provide a use-case demonstration of GeoLCES implementation using data from a recent fire incident.

2. Methods

2.1. GeoLCES Metrics

GeoLCES comprises three distinct but related spatially explicit metrics: (1) visibility index (VI); (2) escape route index (ERI); and (3) proportional safe separation distance (pSSD) (Figure 1). VI quantifies the proportion of firefighters' surroundings that are visible from a given viewing perspective. It ranges from 0 (or 0%; no surroundings visible) to 1 (or 100%; all surroundings visible) [27]. VI is a scale-dependent measure, requiring the definition of a viewing distance within which the VI is to be calculated. ERI quantifies firefighter mobility based on the friction posed by landscape characteristics within one's surroundings [28]. It is calculated as a ratio between the distance one can walk in the presence of extant landscape impediments (e.g., sloping terrain, rough ground surfaces, dense vegetation) and the distance one could walk under ideal conditions (i.e., slightly downhill slope, smooth ground surface, no vegetation). Like VI, it ranges from 0 (or 0%; complete immobility) to 1 (or 100%; highest possible mobility). Also like VI, ERI is scale-dependent; however, whereas VI is defined by a distance (i.e., "how much can I see within a viewing distance of 1000m?"), ERI's scale is defined by an evacuation time frame (i.e., "how far can I walk in 10 minutes?"). pSSD represents the degree to which one is or is not far enough from proximal flames to avoid burn injury [11]. It is the quotient of one's actual distance from fuel and the SSD that one theoretically requires. It is bounded on the low end by 0 (or 0%; no separation from fuel), but practically has no upper bound. Any value equal to or greater than 1 (or 100%) would indicate that one is far enough away from flames to avoid injury.

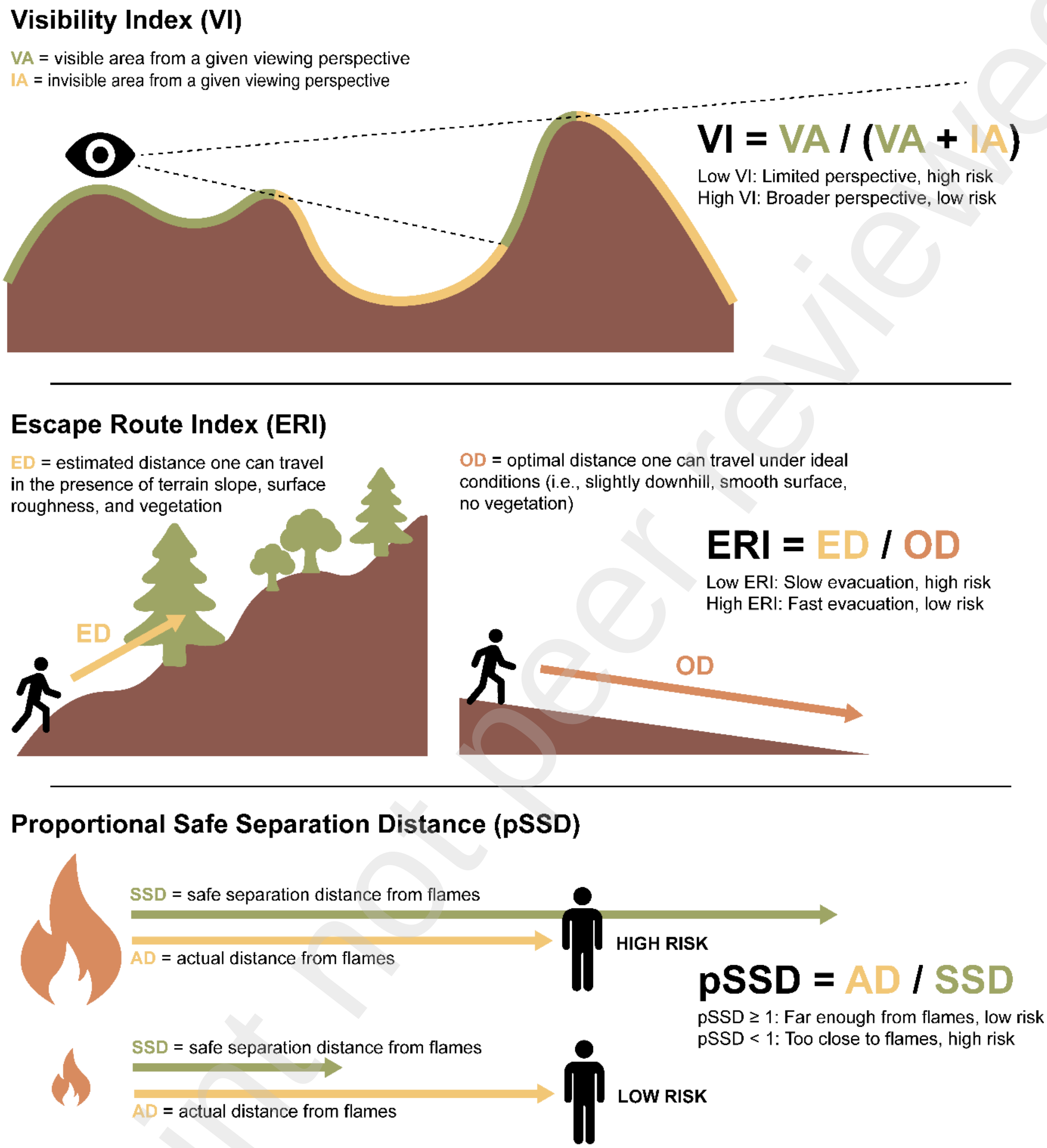

Figure 1. *Graphical representations and basic calculations of the three GeoLCES metrics, including the visibility index (VI; top), escape route index (ERI; middle), and proportional safe separation distance (pSSD; bottom). For simplicity, these metrics are illustrated linearly (i.e., one-dimensionally); however, in a geospatial context, they are computed in two dimensions.*

The following subsections describe each of the three GeoLCES metrics in greater detail, with a focus on their geospatial computation in two-dimensions. They include a thorough discussion of the various considerations one must take into account when generating these metrics to maximize their utility in the context of wildland firefighter safety.

2.1.1. Visibility Index (VI)

To map VI in two dimensions, three things are required: (1) a digital elevation model (DEM); (2) a defined viewing area of interest; and (3) a viewshed algorithm. There are two main types of DEM: (1) digital terrain models (DTMs), which contain per-pixel representations of ground surface elevations; and (2) digital surface models (DSMs), which represent the elevation of the ground plus any aboveground features (e.g., trees, buildings) [29]. DSMs are better-suited for VI calculation, as ignoring aboveground features tends to yield an overly optimistic representation of visibility [30]. Especially in the landscapes within which wildland firefighters tend to work, tall vegetation can hinder visibility well beyond the effects of terrain features alone. DSMs can be generated through the spatial interpolation of airborne lidar first return points, which represent the first surfaces lidar pulses interact with on their path from the aircraft to the ground. An important parameter to consider for this process is spatial resolution, with higher resolutions (i.e., smaller pixels) yielding more accurate visibility estimates, at the expense of computational cost [31].

In geospatial terms, VI is a “focal” measure, meaning it is computed on a per-pixel basis, but it depends on data surrounding each pixel in some pre-defined neighborhood (sometimes referred to as a kernel or moving window) [27]. Accordingly, one must define a neighborhood within which VI calculations are based. Perhaps the most logically consistent neighborhood is that of a circle defined by a viewing radius of interest, as this quantifies how much of one’s surroundings can be seen in all directions within a fixed distance. The most important parameter here is the viewing radius, with smaller distances being more computationally efficient, but only providing quantification of “local-scale” visibility.

Viewshed algorithms typically map visibility in a binary fashion, classifying pixels as either visible or invisible (obscured) from a given viewpoint [32]. If these pixels are encoded as 0 (invisible) and 1 (visible), computing the mean of all pixel values within the focal neighborhood yields VI for the neighborhood’s central (target) pixel. Equivalently, one could divide the total visible area by the total neighborhood area to yield the same VI. Several viewshed algorithms exist, with different software packages implementing different algorithms, but generally they vary primarily in computational efficiency rather than model results, as they are based on the same line of sight geometrics or approximations thereof [33].

Computing VI at operationally useful scales (i.e., hundreds to thousands of hectares) at operationally useful resolutions (i.e., 10m or 30m) can be extremely computationally expensive. One recently developed solution for dramatically increasing the efficiency of broad-scale VI mapping is VisiMod (Figure 2) (Mistick and Campbell 2023; Mistick *et al.* 2023). VisiMod uses a relatively small sample of viewsheds, along with a suite of terrain and vegetation structural predictor variables derived from lidar data, and a random forest modeling framework to generate predictive maps of VI.

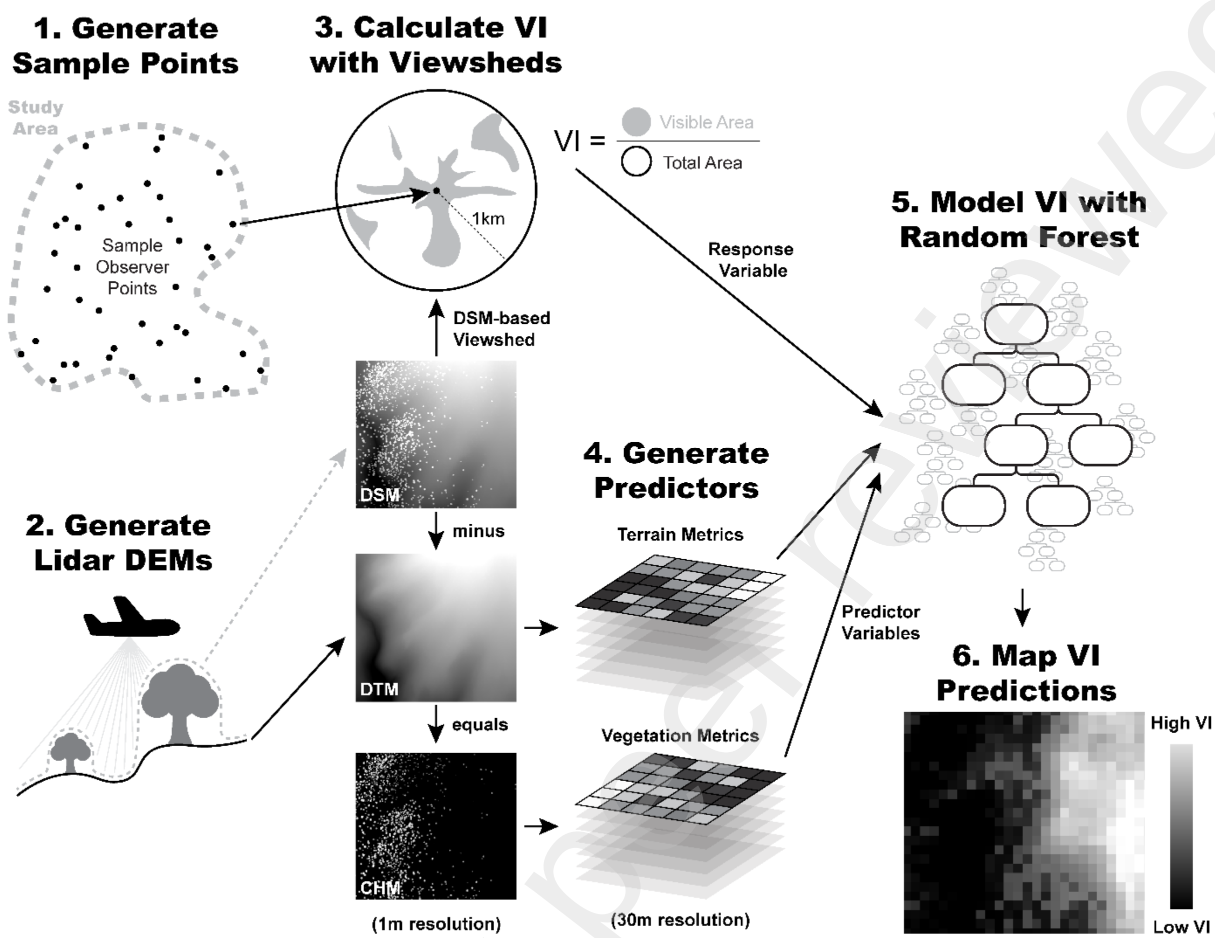

Figure 2. A visual summary of the VisiMod workflow. First, a series of sample points are created within a study area, which will represent the observer points that will be used to train and test the predictive model. Second, airborne lidar-derived digital elevation models (DEMs) are created, including a digital terrain model (DTM), representing terrain elevations, and a digital surface model (DSM), representing terrain plus aboveground feature elevations. Third, the DSM is used to map the viewshed from each sample observer point, and visibility index (VI) is calculated as the ratio of visible area to total area within a viewing radius of interest. Fourth, a suite of terrain and vegetation predictor variables are generated from the DTM and a canopy height model (CHM), which is the difference between DSM and DTM. Fifth, the sample VI values serve as the response variable in a random forest model trained on the vegetation and terrain predictor variables. Lastly, the model is used to map VI predictions across the study area.

2.1.2. Escape Route Index (ERI)

The most important considerations for mapping ERI in two dimensions are: (1) a pedestrian friction surface; and (2) an evacuation time frame of interest [28]. The friction (also referred to as “cost” or “impedance”) surface defines the time required to traverse a pixel on foot, taking into account the various landscape characteristics present within that pixel [36]. Creating a friction surface requires two interdependent elements: (1) an equation that quantifies the relationship between one or more landscape characteristics and travel rates; and (2) spatial representations of those landscape characteristics. Historically, terrain slope has been the most common (and often the sole) variable for defining friction [37]. This is likely attributable to the facts that DTMs, from which slope can be derived, are widely available, and the slope-travel rate relationship has been well-studied. Tobler’s hiking function, for example, can be easily applied to a slope map to create a friction surface [38].

Slope, although certainly important, is not the only landscape characteristic that inhibits pedestrian mobility. Particularly in the environments where wildland firefighters work, there are at least two other variables that must be considered [12,39,40]. The first of these is vegetation density, particularly that within the vertical range occupied by the human body, which plays a major role in reducing travel rates. Lidar is ideally suited to quantifying height range-specific vegetation density. Even under a forest canopy, narrow laser pulses can exploit small canopy gaps, penetrating through to vegetation in the understory and yielding point cloud measurements that capture the structure of low-lying vegetation. Dividing the number of lidar points that fall within a particular height range by the number of points that fall within and below that range produces an estimate of the proportion of lidar pulse energy absorbed in that height range. This metric, referred to as normalized relative point density (NRD), acts as a useful proxy for vegetation density, and has been shown to relate directly to travel rates [12,41].

Secondly, the roughness of unimproved (i.e., off-trail) or partially improved (i.e., hiking trail or containment line) ground surfaces can also act to hinder efficient movement. Roughness represents local-scale deviations (i.e., pits and bumps) from the broader-scale undulations in the terrain surface [42]. Lidar stands alone in its ability to produce DTMs at a high-enough resolution to quantify this microtopography. Indeed, lidar-derived surface roughness has been demonstrated to be a significant predictor of pedestrian travel rates [12,41].

The recently introduced Simulating Travel Rates In Diverse Environments (STRIDE) model enables the accurate prediction of travel rates using lidar-derived slope, vegetation density, and ground surface roughness estimates [41]. In so doing, it represents a viable and relevant solution for generating friction surfaces for ERI calculation. STRIDE is formulated as follows (Eq. 1):

$$t = \frac{\beta_3\left(\frac{1}{\pi\beta_2\left(1+\left(\frac{s-\beta_1}{\beta_2}\right)^2\right)}\right)}{1+\beta_4 d+\beta_5 r} \tag{1}$$

where t is travel rate in m/s, s is terrain slope in degrees, d is vegetation density approximated by NRD (unitless ratio), r is ground surface roughness in m, and β_1, …, β_5 are model coefficients empirically determined by Campbell *et al.* (2024).

Beyond these three landscape variables, which affect movement on a continuous basis, it is useful to consider barriers, through which pedestrian travel is prohibited. These can include features such as waterbodies, buildings, and impassibly steep slopes. If generated in real or near-real time on a fire incident, then the fire perimeter (and perhaps some buffer around it to account for potential spread) could also be considered a barrier [20].

Like VI, ERI is a focal measure, computed on a per-pixel basis, but dependent upon friction surface data within a surrounding neighborhood. Unlike VI, whose neighborhood is defined by a viewing distance, ERI's neighborhood is defined by a travel time, representing a simulated evacuation time frame (e.g., 10 minutes). To map ERI across an entire study area of interest, then, each pixel in that area represents a potential evacuation starting point (i.e., a fire crew's position on the landscape at any given time) (Figure 3). Total accumulated travel time radiating outward from that starting point is computed according to the friction surface and a least-cost path algorithm that minimizes travel time to each sequentially adjacent pixel. This accumulation process is terminated when the target travel time is reached, yielding an isochrone that represents the distance one can travel, in all directions, from the starting point within the defined evacuation time frame. A separate isochrone, representing the distance one could travel under ideal landscape conditions (i.e., the maximum travel rate possible with the STRIDE model) is also computed. The mean of linear distances between the starting point and the “actual” isochrone (that takes STRIDE-based friction into account), and that between the starting point and the “optimal” isochrone (that maximizes STRIDE-based travel rates) yields the ERI. This process is repeated for every pixel on the landscape, yielding a map that represents proportional mobility, given surrounding conditions, within a simulated evacuation time frame.

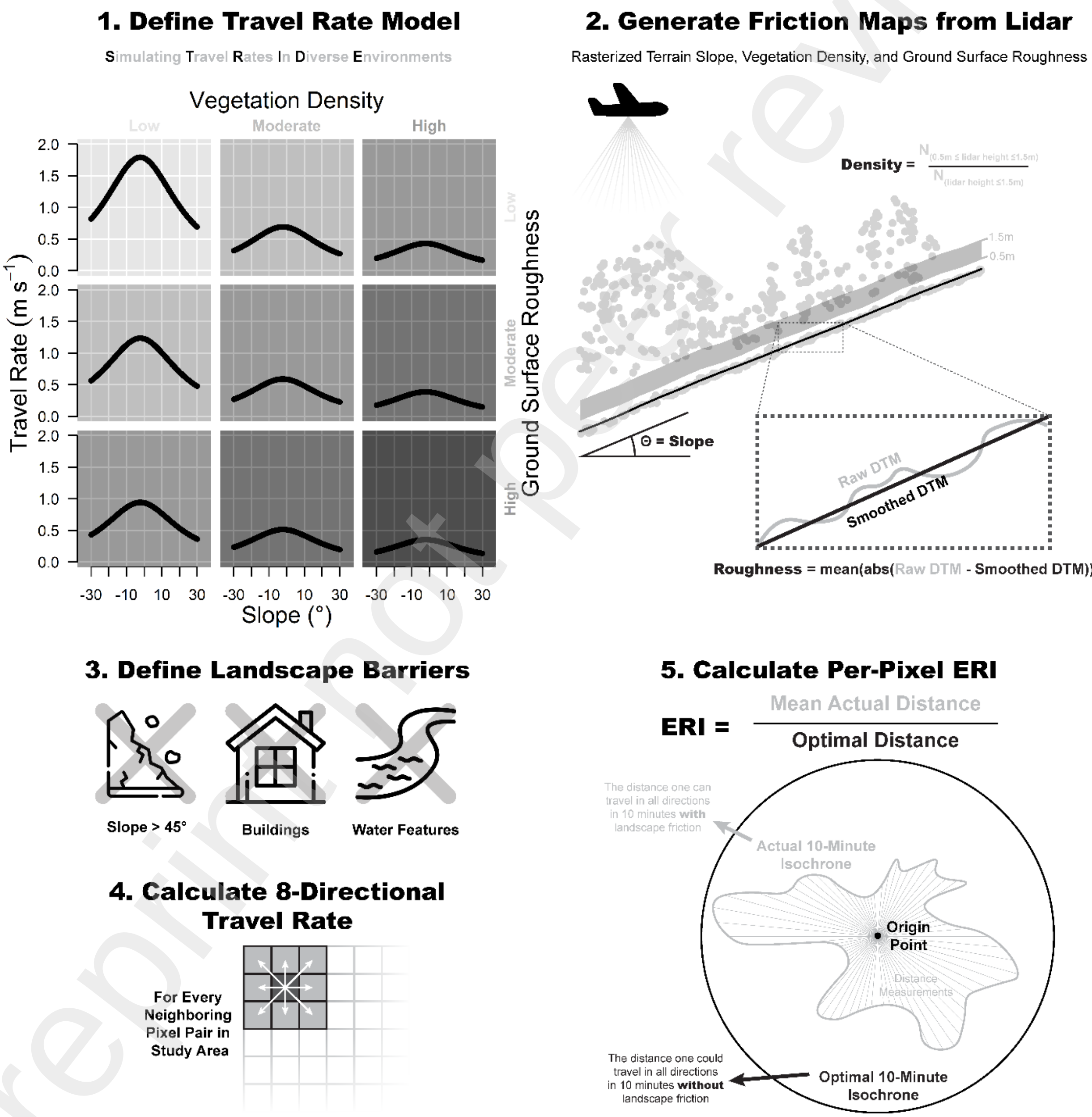

Figure 3. *A visual summary of the Escape Route Index (ERI) workflow. First, a travel rate model is defined; in our study, we have defined this with the Simulating Travel Rates In Diverse Environments (STRIDE) model, which accounts for slope, vegetation density, and ground surface roughness in estimating travel rates. Second, these three landscape variables are mapped using*

airborne lidar. Third, barrier maps are generated, representing impassible landscape features. Fourth, a transition matrix is generated by calculating the travel rate between all adjacent pixels in the study area. Lastly, from each cell in the study area, the mean distance to a 10-minute evacuation isochrone is divided by the optimal distance one could travel in the absence of landscape impediments, yielding per-pixel ERI.

2.1.3. Proportional Safe Separation Distance (pSSD)

The current method for calculating SSD – the minimum distance needed to avoid burn injury – is based on two heat transfer mechanisms: radiation and convection. The radiation component is addressed using a simple rule of thumb, where SSD is equal to or greater than eight times the height of nearby vegetation. This is based on the work of Butler and Cohen (1998), who determined that SSD should be equal to or greater than four times the height of nearby flames [22]. Given that safety zones should be evaluated pre-fire (i.e., before flame heights can be directly visually assessed), a simple assumption that, in a crown fire, flame heights will be approximately twice vegetation height yields the eight times vegetation height guideline.

However, in the presence of steep slopes, high winds, and under more intense burning conditions driven by heavy fuel loads, exceedingly dry fuels, and/or low relative humidity, convective heat can significantly increase SSD. To account for this, the work of Frankman *et al.* (2012), Gallacher *et al.* (2018), Butler *et al.* (2019) and others have yielded multiplicative factors, often represented by Δ, that should be multiplied by the radiative eight times vegetation height to yield a safer and more realistic SSD (Eq. 2; Table 1) [43–45]:

$$SSD = 8 \times h \times \Delta \tag{2}$$

where h is vegetation height in m, and Δ is a multiplicative factor from Table 1.

Table 1. *Multiplicative factors (Δ) to be used in Eq. 2 for accounting for the effects of convective heat transfer under varying fuel, weather, and topography conditions [46].*

Wind Speed (m/s)	**Burning Conditions**	**Slope (%)**		
		Flat (0-25)	*Moderate (25-45)*	*Steep (>45)*
Light (0-4.5)	*Low*	1	1	2
	Moderate	1	1	2
	Extreme	1	2	3
Moderate (4.5-8.9)	*Low*	1.5	3	4
	Moderate	2	4	5
	Extreme	2.5	5	5
High (>8.9)	*Low*	3	4	6
	Moderate	3	5	7
	Extreme	4	5	10

To map pSSD in two dimensions requires first that SSD is mapped on a per-pixel basis. Two of the four variables that contribute to SSD estimation (vegetation height and terrain slope) are static, and can be readily mapped at pixel scales using lidar data. The other two (wind speed and burning condition) are dynamic, and thus cannot be reflected in a singular, static geospatial metric. However, a Δ parameter based on wind speed and burning condition can be used to scale per-pixel SSD according to expected fire conditions [11].

Mapping pSSD also requires the identification of a vegetation height threshold. Pixels with vegetation height below this threshold can serve as a safety zone. Areas entirely devoid of fuel are ideal for safety zones, but may not exist in sufficient abundance to be useful. Therefore, including areas with short (e.g., <1m) vegetation that could either be cleared mechanically or burned out will yield a more inclusive, and ideally more realistic, set of potential safety zones.

Once SSD is mapped on a per-pixel basis with a fixed set of wind speed and burning condition parameters, pSSD can be mapped within the areas defined as being potential safety zones (below the aforementioned vegetation height threshold). This is done using Eq. 3:

$$pSSD_i = \min_{j \in P} \left(\frac{d_{ij}}{SSD_j} \right) \tag{3}$$

where $pSSD_i$ is the pSSD for one pixel i that falls within a potential safety zone, d_{ij} is the Euclidean distance between pixel i and pixel j, SSD_j is the SSD for pixel j, and j belongs to a set of pixels P, which encompass all pixels in a study area outside of the potential safety zone (i.e., taller vegetation pixels that contribute to pSSD calculation). Pixels with a pSSD value over one are expected to have sufficient distance from burning vegetation to minimize harmful radiant and convective heat exposure. As pSSD decreases from one, the potential for threatening heat exposure increases. In any case, pSSD should be maximized when assessing safety zone suitability.

To run a pSSD calculation iteratively for every pixel in a study area would be very time-consuming, even with parallelization. One way to substantially reduce processing time is to bin the SSD values into classes (e.g., 0-10m, 10-20m, etc.), iterate through the groups of pixels belonging to those classes, map Euclidean distance from those pixel groups, and divide by the midpoint of the bin range (e.g., 5m, 15m, etc.).

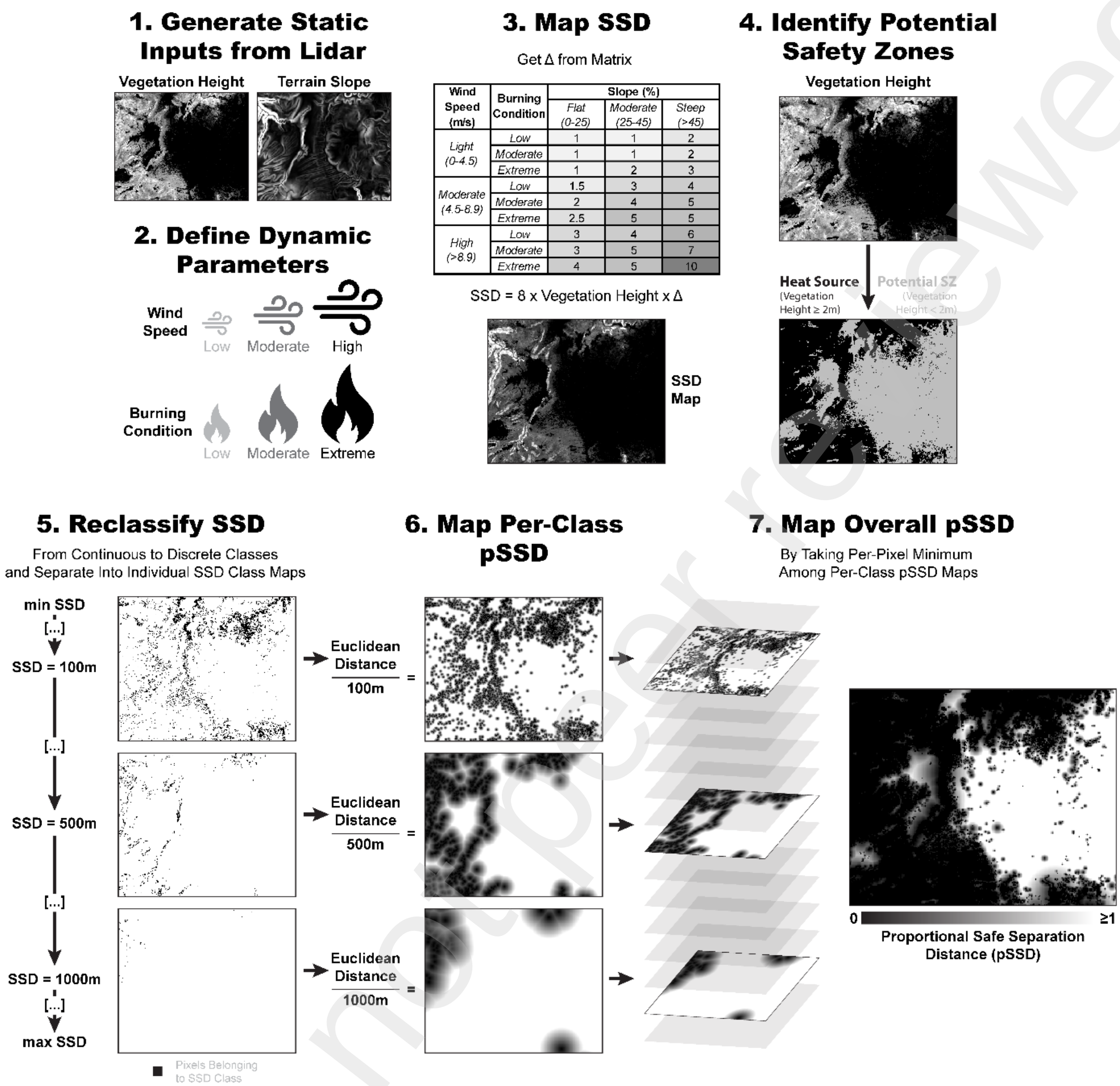

Figure 4. *A visual summary of the proportional safe separation distance (pSSD) workflow. First, vegetation height and terrain slope maps are derived from airborne lidar data. Second, wind speed and burning condition are parameterized. Third, these four inputs are used, along with the multiplicative factor (Δ) matrix to map safe separation distance (SSD) on a per-pixel basis. Fourth, potential safety zones are identified, based on a vegetation height threshold. Fifth, SSD is reclassified and separated into a series of individual SSD maps. Fifth, pSSD is mapped from each class-specific SSD map by dividing Euclidean distance from pixels belonging to the SSD class by the SSD value. Lastly, the per-pixel minimum among all class-specific pSSD maps is computed to yield the final pSSD map, representing the degree to which pixels are or are not far enough from nearby fuel to avoid burn injury.*

Firefighter safety will be maximized in areas with high pSSD, ERI, and VI. Low values of any one of these metrics can indicate compromised firefighter safety.

2.2. GeoLCES Demonstration

2.2.1. Data and Study Area

To demonstrate the application of GeoLCES on a scale that would be useful for operational fire management purposes, we selected Gila National Forest in New Mexico, USA as a study area. The Gila National Forest is well-suited for demonstrative purposes for a variety of reasons, including its fire-prone nature, diversity of terrain conditions and fuel types, large size, and the free, forest-wide availability of recent airborne lidar data. Situated in the southwestern portion of New Mexico, the National Forest encompasses 13,716 km^2 in area, making it the 12th largest National Forest in the contiguous US. The Forest contains a large elevation range (1,264 – 3,318m), which drives large annual mean temperature (4 – 15°C) and precipitation (298 – 1089mm) gradients. The dominant vegetation types tend to follow these environmental gradients, with lower, warmer, and drier areas being dominated by sparse, xeric grasslands and shrublands, transitioning to denser chaparral and encinal shrub-woodland mixtures, dry conifer woodlands and parklands, and more mesic mixed coniferous-deciduous forests at the highest elevations, with montane shrublands and meadows interspersed throughout. According to USDA Forest Service Forest Inventory and Analysis (FIA) data, the most common tree species found in Gila National Forest is Ponderosa pine (*Pinus ponderosa*; 22% of recorded trees in the FIA database), followed by common piñon (*Pinus edulis*; 22%), alligator juniper (*Juniperus deppeana*; 14%), Gambel oak (*Quercus gambelii*; 11%), Arizona white oak (*Quercus arizonica*; 6%), Douglas-fir (*Pseudotsuga menziesii*; 6%), gray oak (*Quercus grisea*; 6%), oneseed juniper (*Juniperus monosperma*; 2%), silverleaf oak (*Quercus hypoleucoides*; 2%), and white fir (*Abies concolor*; 2%) [47].

The primary data source needed to successfully demonstrate GeoLCES was airborne lidar data. We acquired lidar data covering Gila National Forest from the United States Geological Survey (USGS) 3D Elevation Program (3DEP) (Table 2) [48]. To account for the fact that ERI and VI are focal measures, we buffered Gila National Forest's administrative boundary by 1km, and downloaded every tile of lidar data available within that buffered area. In all, that comprised data 7,171 tiles of data from seven different 3DEP datasets (referred to as "work units", representing individual airborne campaigns). With the exception of the proportionally small AZ_USFS_3DEP_Processing_2019 dataset which was collected in 2013-2014, the data were collected between 2018-11-20 and 2019-06-06. The mean pulse density, weighted by work unit area, among all of the lidar datasets used in this study was 4.55 pulses/m^2, which yielded an average weighted point density of 6.50 points/m^2. In all, these data contained over 102 billion lidar points, occupying over 4 TB of disk storage, even with the highly compressed LAZ file format.

Table 2. *Airborne lidar datasets acquired and processed for the demonstration of GeoLCES within Gila National Forest.*

Work Unit	Start Date	End Date	Tile Count	Area (km^2)	Point Density (pts/m^2)	Pulse Density (pls/m^2)
AZ_USFS_3DEP_Processing_2019	2013-08-24	2014-10-12	97	74	21.33	16.58
NM_SouthCentral_B10_2018	2019-04-18	2019-06-06	1,156	2,601	5.50	3.37
NM_SouthCentral_B2_2018	2018-11-21	2019-02-01	236	531	6.43	6.15
NM_SouthCentral_B3_2018	2018-11-20	2019-05-27	1,152	2,545	7.39	4.92
NM_SouthCentral_B5_2018	2018-12-30	2019-05-30	144	324	7.03	5.02
NM_SouthCentral_B7_2018	2018-12-04	2019-05-26	210	457	4.86	3.38
NM_SouthCentral_B8_2018	2018-11-20	2019-06-06	4,126	9,208	6.49	4.63

All lidar data processing took place in *R* v4.4.1 using the *lidR* package v4.1.2 [49,50]. Processing was done first at the level of the individual lidar tile, then mosaicked to the level of the work unit (Table 2), which was, in turn, mosaicked across the entire study area. If reprojection was needed (as work units are delivered with different coordinate reference systems), bilinear resampling was employed. Prior to any lidar processing (Section 2.2.2), points flagged as withheld or classified as noise were removed from consideration.

VI and pSSD are solely dependent upon lidar data; however, ERI can benefit from the inclusion of barriers supplied by additional datasets. For this study, we also acquired hydrography data from the National Hydrography Dataset and Microsoft building footprints, both of which were used to map impassible landscape features when simulating pedestrian travel (the process for which is described in Section 2.2.2) [51,52].

2.2.2. GeoLCES Metric Mapping and Analysis

To map VI across the entire study area at a 30m resolution, we used *VisiMod* v2.0 in *R* (Figure 2) [34,35,50]. *VisiMod* requires a DTM, representing terrain elevations on a per-pixel basis, and a DSM, representing terrain plus aboveground feature height. We generated the DTM and DSM at 1m-resolution from the airborne lidar. The DTM was created using triangulated irregular network-based interpolation of lidar points classified as ground returns (*rasterize_terrain()* function in *lidR*, with the *tin()* algorithm). The DSM was generated using the *pitfree()* algorithm in the *rasterize_canopy()* function. *VisiMod*'s main parameters include: (1) the number of points used to train and validate the random forest VI prediction model (we selected 10,000); (2) the distance (viewing radius) within which to model VI (we selected 1km); (3) the aggregation factor, representing a multiplier that defines the resolution of the predictor variables and output VI map (we selected 30); and (4) whether VI is omnidirectional or directionally specific (we selected omnidirectional, i.e., 360° field of view). We tuned the *VisiMod* random forest model's hyperparameters (as implemented in the *ranger* v0.16.0 package in *R*) using the model-based optimization provided in the *tuneRanger* v0.7 package [53,54]. We assessed the performance of the model using a spatial 10-fold cross-validation, where Gila National Forest was first subdivided into 10 evenly sized polygons split along the north-south axis. Iteratively, points that fell within each fold polygon were set aside for validation as points from the other nine-fold polygons were used to train a model. Each trained model was applied to the prediction of VI for points in its respective validation fold, the compilation of which yielded 10,000 predicted versus observed VI values, which we used to quantify R^2, RMSE, and bias. A final random forest model was also built using all 10,000 observations as training data, which was used to map VI across the entire study area.

To map ERI study area-wide, we generated several input variables using the *terra* v1.8.5 and *lidR* packages in *R*, each mapped within a 1km buffered area around Gila National Forest's boundary at 30m spatial resolution (Figure 3) [49,50,55]. Given that we were relying on the STRIDE model (Eq. 1) as the primary basis of assessing landscape friction, we needed three lidar-derived inputs: (1) a DTM, which served as the basis for directionally specific slope calculation; (2) an NRD raster, which represented vegetation density; and (3) a ground surface roughness raster. The DTM was simply generated through the mean aggregation of our lidar-derived 1m-resolution DTM to 30m. The NRD raster was computed as the number of lidar points within the aboveground height range of 0.5 – 1.5m divided by the number of points 1.5m and below within each 30m pixel in the study area. The roughness raster was calculated as the 30m aggregate mean of the absolute difference between a 1m DTM and a DTM smoothed using a 2m-radius circular focal mean. We also generated three 30m "barrier" rasters, representing impassible landscape features. The first represented areas with slopes steeper than 45°, derived from the 30m DTM. The second represented impassible waterbodies, which we derived from National Hydrography

Dataset waterbodies and area features[51]. The third represented built structures, which we derived from the Microsoft Building Footprints dataset [52].

Using these friction and barrier surfaces, we created a transition matrix using the *R* package *gdistance* v1.6.4, which quantifies the conductance between every adjacent 30m cell, in eight directions, throughout the study area [56]. We used the STRIDE model (Eq. 1) as the basis for computing pixel-to-pixel conductance, with coefficients from Campbell *et al.* (2024)'s model based on an NRD height range of 0.5 – 1.5m (β_1 = -2.196; β_2 = 25.453; β_3 = 143.410; β_4 = 4.502; β_5 = 15.868) [41]. Using this transition matrix, we generated per-pixel 10-minute travel time isochrones radiating outward from every 30m pixel in the study area. The mean distance from the center origin pixel to the isochrone pixels was divided by 1076 m, yielding the per-pixel ERI values. This number came from the optimization of Eq. 1, yielding the idealized travel rate of 1.79 m/s, where slope is slightly downhill (-2.2°), and vegetation density and roughness are both set to 0.

To map pSSD at 30m resolution study area-wide, we first needed to map vegetation height (Figure 4). We did this by differencing the lidar-derived, 1m resolution DTM and DSM datasets, yielding a 1m resolution canopy height model. To aggregate to 30m, we took the 95th percentile canopy height within each 30x30 pixel area. We opted for the 95th as it minimized the potential noise that might be inherent to using the maximum value, while still trying to capture the height of the tallest vegetation within each aggregation area. Pixels with a 95th percentile vegetation height less than 1m were considered to be potential safety zones (within which pSSD was to be mapped), whereas pixels greater than or equal to 1m were considered heat sources (from which SSD was to be calculated). We mapped slope at 30m resolution from the previously generated 30m DTM. With slope and vegetation height mapped, we needed to select wind speed and burning condition classes to use as the basis of GeoLCES demonstration. For GeoLCES demonstrative purposes, we chose moderate wind speed (4.5 – 8.9 m/s) and moderate burning condition (Table 1). SSD was computed for every pixel according to Eq. 2, yielding a per-pixel representation of the distance one would need to maintain from each pixel to avoid burn injury. To map pSSD, we reclassified the SSD values by rounding to the nearest 10, iterated through each class, and computed pSSD from pixels belonging to that class using Eq. 3. The minimum among all resulting pSSD rasters within the potential safety zones was calculated on a per-pixel basis, representing the final pSSD map.

Once all three GeoLCES metrics were mapped study area-wide, we analyzed them in a few different ways. First, to understand the relationship between inputs and outputs, we compared ERI, VI, and pSSD qualitatively and visually to a selection of their primary input datasets, including elevation, canopy height, and vegetation density (as approximated by NRD). Second, we compared the three metrics to one another on a per-pixel basis to assess how correlated they might be to one another. Third, to understand vegetation type-level differences in them, we compared the three metrics to the 2020 LANDFIRE Existing Vegetation Type, including analyses of variance that sought to determine what proportion of each metric's variance could be explained by vegetation type alone [57].

2.2.3. Visualization and Interpretation

As one of the primary objectives of this research is to unite three separate spatial metrics to facilitate a simultaneous, holistic, and multivariate evaluation of firefighter safety, we needed to devise a strategic visualization approach that could be used to represent GeoLCES graphically. To this end, we leveraged the three display channels of color imagery: red, green, and blue. Specifically, we assigned ERI to the red channel, VI to the green channel, and pSSD to the blue channel (Figure 5). Thus, the brightness levels of these individual display channels correspond to the magnitude of pixel values in each of the three firefighter safety metrics. The benefit of this visualization approach is that the unique color combinations that emerge can provide useful insights into the spatial dimensions of all three metrics at once (Table 3). The drawback of this approach is that users with some form of color vision limitation may not be able to discern different hues and associate those hues with their fire management implications. To address this limitation, we also generated visualizations of the three metrics individually using accessible color schemes.

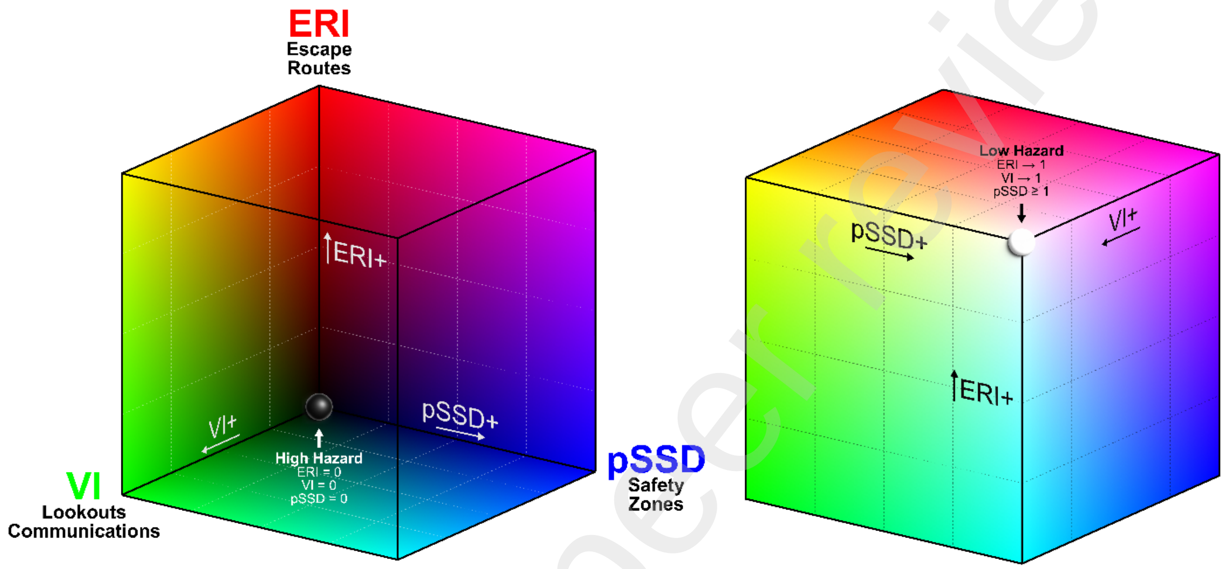

Figure 5. *Three-dimensional representation of the three GeoLCES metrics displayed as brightness levels along red (escape route index; ERI), green (visibility index; VI), and blue (proportional safe separation distance; pSSD) axes. Where the three values are mapped as having values approaching or equal to zero, these areas may represent high hazard areas for wildland firefighters (left). Where the three values are high, these areas may be comparably low hazard (right).*

Table 3. *A selection of colors that can result from displaying the three GeoLCES metrics through the red, green, and blue (RGB) display channels of a color image, including the relative magnitude of each metric that would yield the color, and the possible fire management interpretation of the color. Note that the relative terms "high" and "low" are used in lieu of exact values for the three GeoLCES metrics, as end users can determine what thresholds are relevant for their focal landscape and fire regime.*

Color	ERI (R)	VI (G)	pSSD (B)	Interpretation
Black	Low	Low	Low	Low egress, visibility, and fuel separation gives these areas the highest hazard potential, making them unsuitable for any firefighting activities
White	High	High	High	High egress, high visibility, and fuel separation gives these areas the lowest hazard potential, making them suitable for all firefighting activities
Red	High	Low	Low	High egress, but low visibility and fuel separation means these areas may be suitable for a ground crew to be located; however, it would be essential that they are within a close proximity to an area with high pSSD (for safety zone access) and in close communication with a lookout with high VI (to provide situational awareness by proxy).
Green	Low	High	Low	High visibility, but low egress and fuel separation means these areas may be suitable for placement of a lookout; however, this

				lookout would need to be far removed from the active fire, as their ability to evacuate may be limited, and they are too close to nearby fuels.
Blue	Low	Low	High	High fuel separation, but low egress and visibility means these areas may be suitable for safety zones; however, their limited mobility may limit their accessibility and increase risk of injury. If selected for use as a safety zone, these areas would benefit from close communication with a lookout who has high visibility to understand proximal changes in fire behavior.
Cyan	Low	High	High	High visibility and fuel separation, but low egress means these areas may be suitable for safety zones, but may pose safety risks due to the presence of terrain features (e.g., scree fields, steep alpine areas, etc.) that inhibit within-safety zone mobility.
Magenta	High	Low	High	High egress and fuel separation, but low visibility means these areas may be suitable for most fire management activities; however, it would be essential to maintain active communication with a lookout who can provide situational awareness by proxy, given the crews' potentially limited landscape visibility.
Yellow	High	High	Low	High egress and visibility, but low fuel separation means these areas may be suitable for a ground crew to engage in direct or indirect attack; however, it is important that they are sufficiently close to a safety zone with high fuel separation that could serve as an evacuation destination.

2.2.4. Operational Use-Case Demonstration

To provide an example of how GeoLCES could be used in a specific operational context, we acquired National Interagency Fire Center (NIFC) incident data from a fire that occurred within the study area in 2021. The Doagy Fire burned 51.7km^2 between 14 May 2021 and 3 June 2021. We selected this fire for its data availability and its occurrence the year after most of our study area's lidar data were flown, making our GeoLCES maps representative of pre-fire conditions. Using the fire's final containment line, divided into three divisions by division break point data, we extracted ERI pixel values to quantify proportional mobility at point locations every 30m along the line. To quantify proportional visibility both along the line and within a distance of the line where a lookout might be situated, we computed maximum VI within a 500m buffer of the same set of point locations. We also thresholded the pSSD map to pixels greater than or equal to 1, representing potentially viable safety zones, and calculated Euclidean distance to the nearest safety zone for each point along the containment lines as well. We demonstrated how, with these three pieces of information, firefighters could make informed management decisions by understanding the hazard potential of their containment lines. For example, areas with high mobility, visibility, and proximity to a safety zone may be most appropriate to send a hand crew, whereas areas with opposing and potentially dangerous conditions could be avoided by ground personnel, or additional safety measures put in place.

3. Results

The *VisiMod* model for predicting VI performed well, with 71% of variance in observed VI being explained by the model (Figure 6). Furthermore, the model featured very low prediction error (RMSE = 0.02). As is often the case with machine learning models, an ordinary least squares regression between predictions and observations yielded a trendline suggesting the model tended to underestimate high values. However, across the full range of observations, the mean bias was effectively zero, suggesting a balance of over- and underestimation. Observed VI was generally quite low, featuring a heavily positively skewed distribution, with relatively few areas featuring VI greater than 0.2 (or 20%). In this mountainous and heavily vegetated study area, these results suggest that it is rare to be able see more than 20% of one's surroundings within a viewing radius of 1km.

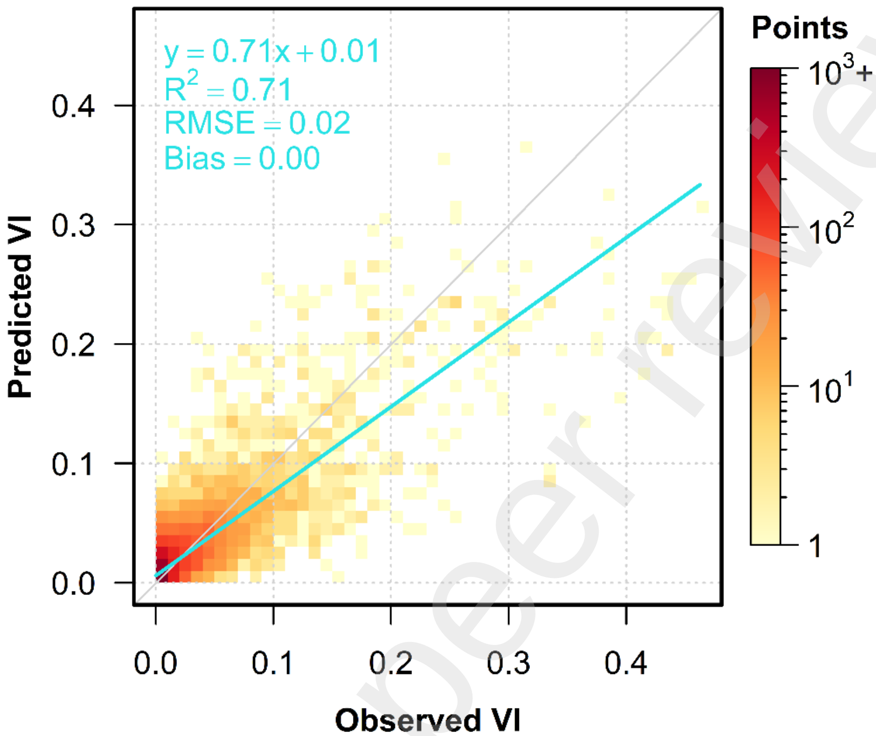

__Figure 6.__ Predicted (y) versus observed (x) visibility index (VI) derived from VisiMod. The predictions and observations are derived from a 10-fold spatial cross-validation procedure where the study area was split into 10 evenly sized subset areas and, iteratively, points that fell within each subset area/fold were set aside for validation while the remainder were used to train a model. To facilitate visual interpretation, the point values were converted to density and displayed using a log scale.

Figures 7 and 8 depict the three GeoLCES metrics mapped across the study area at 30m spatial resolution, with the former leveraging the three-band RGB image compositing approach described in Figure 5 and Table 3, and the latter conveying the metrics separately to facilitate interpretation for those with color vision limitations. There are very clear spatial patterns of areas that promote or hinder wildland firefighter safety. In the RGB visualization, pixels that appear white or nearly so represent the best-case scenario from a safety perspective, with high egress, visibility, and fuel separation. The northern half of the study area features more of these safe areas than the southern half. Focus Area 1 highlights one such example, which could serve as a potential safety zone for wildland firefighters, given the large fuel separation, ease of pedestrian travel, and high visibility (Figures 7 and 8). This area appears to be a large herbaceous area surrounded by forests, containing flat slopes, and short, sparse vegetation – ideal conditions for promoting firefighter safety (Figure 9).

The rugged Mogollon Mountains and Black Range in the southern portion of the study area tend to yield higher-hazard conditions, with generally steeper slopes and denser, taller vegetation limiting both mobility and fuel separation. One example of this can be found in Focus Area 2, which is centered by Mogollon Canyon, a steep and rocky canyon that features very dense vegetation (Figure 9). Despite the low mobility and fuel separation, Focus Area 2 features a relatively high degree of visibility. This is attributable to the abundance of high-relief areas (e.g., canyon rim, knife ridges, cliffs), atop which one could maintain a high degree of visibility; however, their inaccessibility may limit their utility as useful lookout points. Focus Area 3 features an interesting mix of firefighter safety conditions, with cyan pixels suggesting a relatively high degree of visibility and fuel separation and a relatively low degree of mobility. This combination results from the low-stature but very dense vegetation in the chaparral shrubland vegetation found in this area. The vegetation is short enough to facilitate visibility and require relatively short SSDs, but dense in the height range most pertinent to pedestrian movement, reducing the ERI.

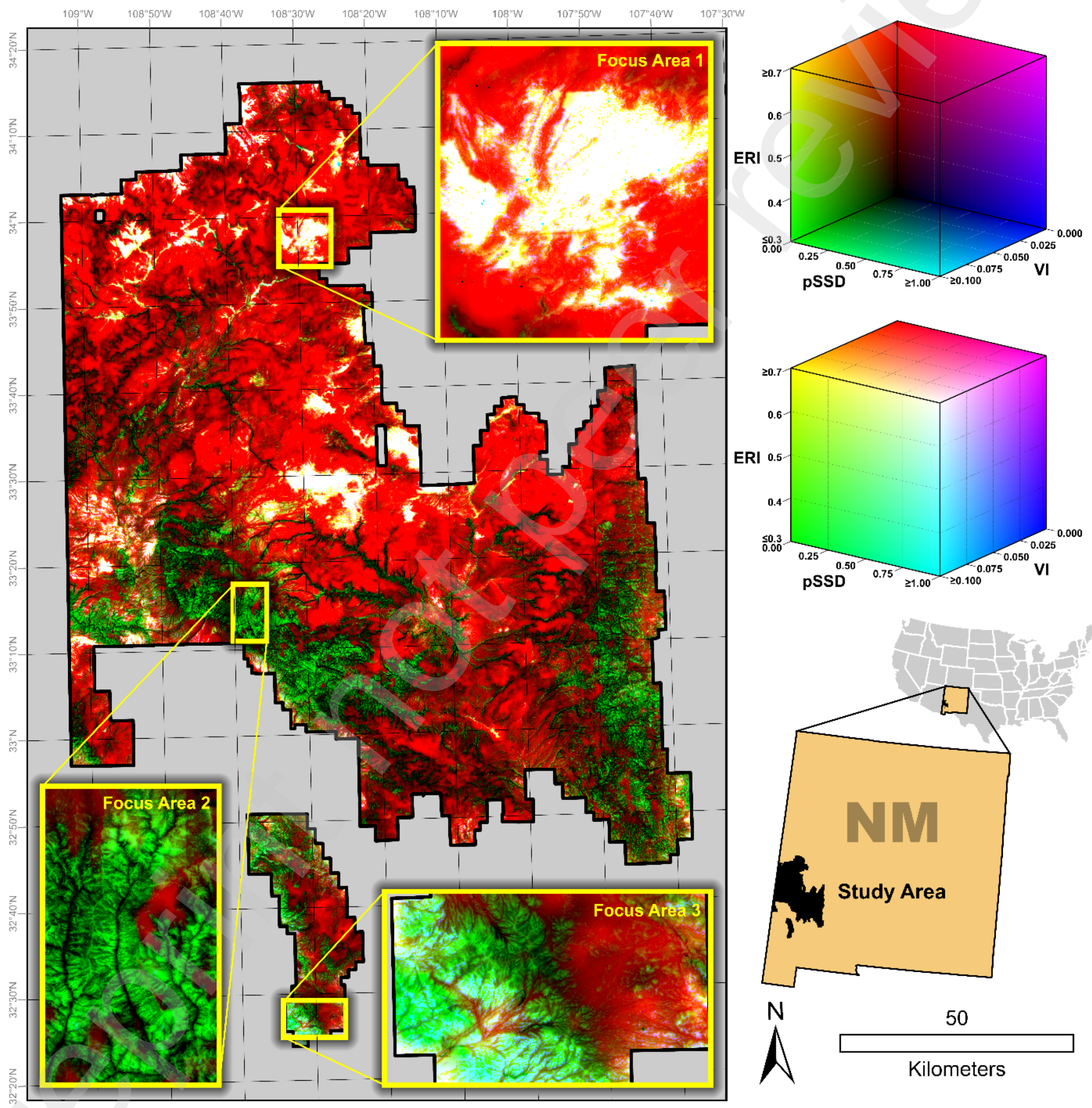

Figure 7. *Results map illustrated using the three-band red-green-blue (RGB) color image visualization approach, where the escape route index (ERI) is displayed through the red channel, the visibility index (VI) is displayed through the green channel, and the proportional safe separation distance (pSSD) is displayed through the blue channel. The two RGB cube legends in the top right provide the ability to interpret the magnitudes of the three metrics that produce specific colors on the map. Three focus areas are shown as inset maps to highlight noteworthy metric combinations.*

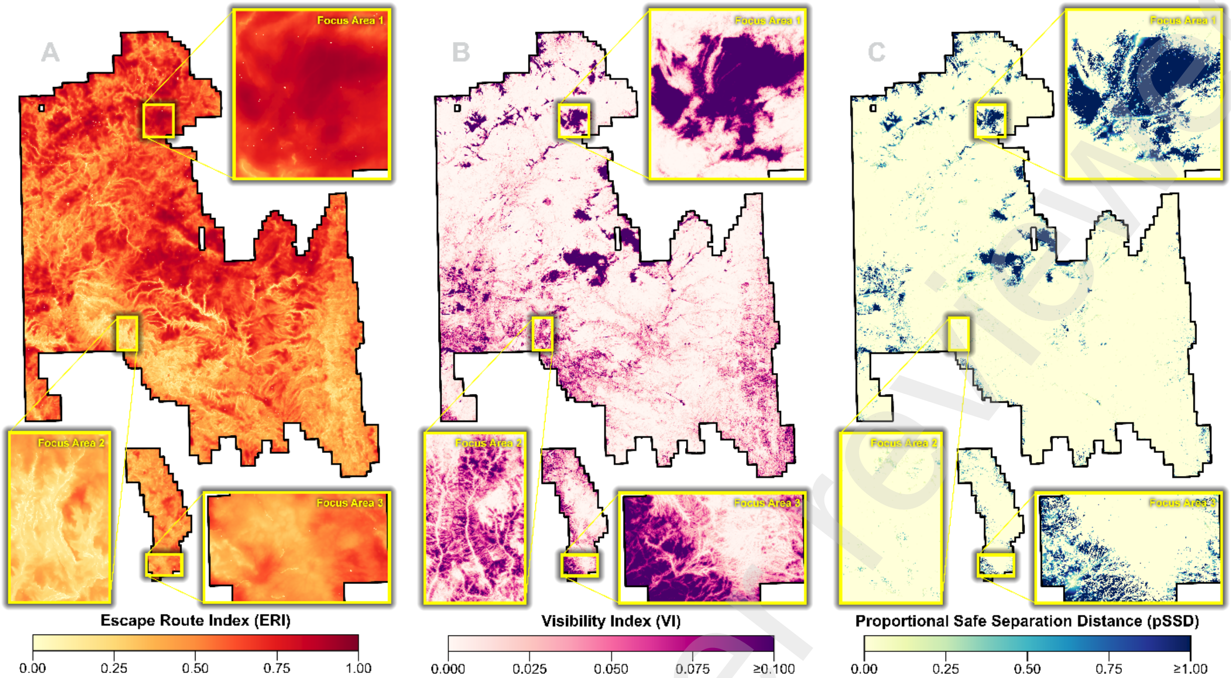

Figure 8. *Separate GeoLCES metric result maps conveyed with accessible color schemes, including: (A) escape route index (ERI); (B) visibility index (VI); and (C) proportional safe separation distance (pSSD). The same three focus areas shown in Figure 7 are shown here to facilitate direct comparison.*

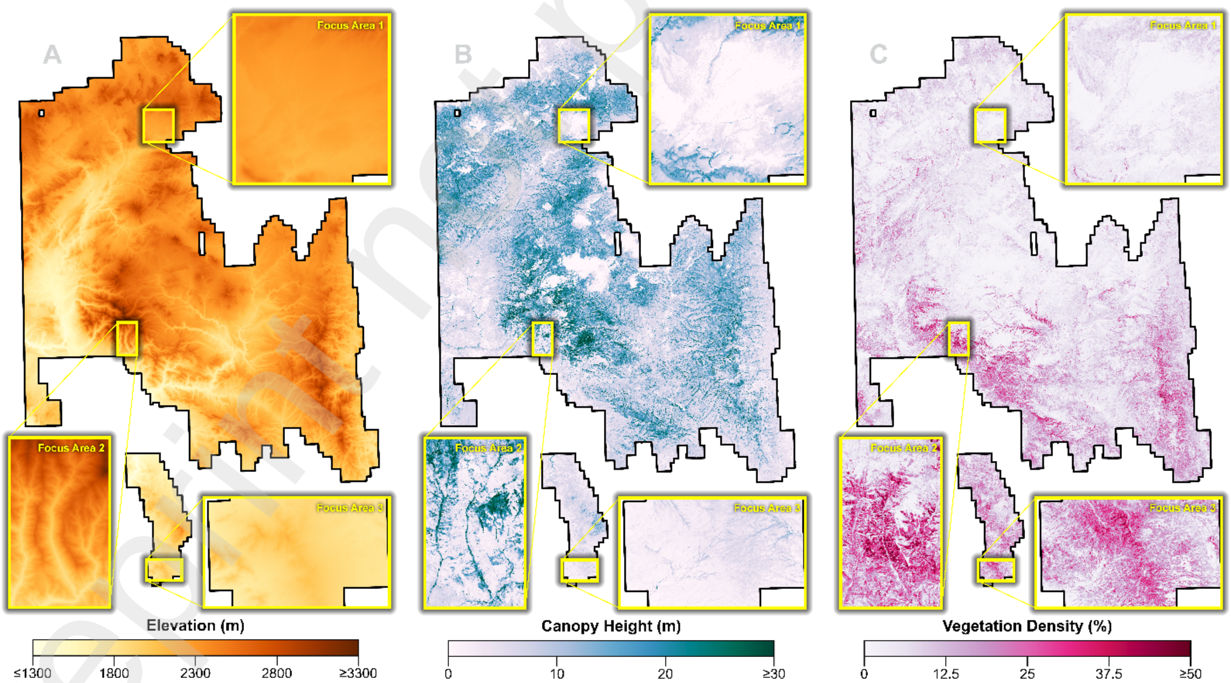

Figure 9. *Three landscape metrics that served as important inputs to, and can help facilitate the understanding of, the three GeoLCES metrics, including: (A) elevation; (B) canopy height; and (C) vegetation density (as approximated by lidar normalized relative density, NRD). The same three focus areas shown in Figures 7 and 8 are shown here to enable comparisons.*

Spatially, VI and pSSD appeared to be highly correlated (Figures 7 and 8). A per-pixel, study area-wide quantitative comparison of the three metrics confirmed this qualitative assessment (Figure 10). Indeed, VI and pSSD featured a Pearson's correlation (r) of 0.75, demonstrating a clear positive trend between the two metrics. This correlation makes intuitive sense – areas that featured high pSSD (i.e., potential safety zones) tended to be large, open areas that contained short and/or sparse vegetation. Naturally, these areas also featured a higher degree of visibility, particularly given that VI in this study was calculated within a viewing radius of 1km. Furthermore, both VI and pSSD featured highly positively skewed distributions – pSSD more so than VI – with relatively few pixels featuring high index values and the vast majority being at or near zero. Given that this analysis was conducted within a National Forest, where the majority of the landscape was vegetated and much of it forested, both visibility and fuel separation, on average, tend to be quite low. This highlights the value of mapping these metrics in advance of a fire, to be able to identify the relatively rare portions of the landscape where visibility and fuel separation are high.

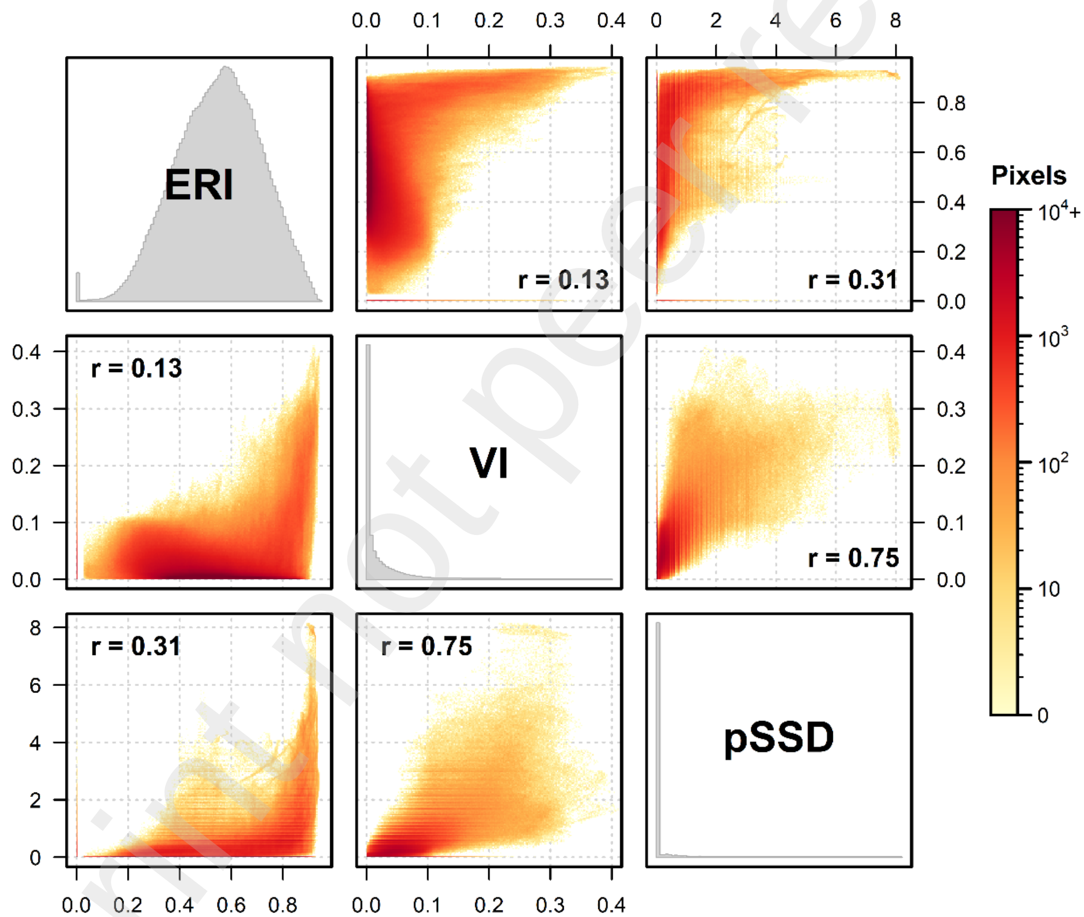

Figure 10. Pairs plot displaying univariate and bivariate distributions of the three GeoLCES variables: escape route index (ERI), visibility index (VI), and proportional safe separation distance (pSSD). The bivariate distributions are displayed according to the number of pixels that fell within binned values of the paired variables. The bin resolution for each plot was 200x200. For clarity, given the highly skewed distributions that resulted, the pixel count was clamped to a maximum of 10,000 and displayed using a log scale.

ERI featured a much more normal distribution, with a mean value of approximately 0.55, suggesting that, on average, traveling through the study area was approximately half as efficient as traveling in an idealized landscape with minimal friction. ERI and pSSD were somewhat correlated (r = 0.31), though considerably less so than VI and pSSD. The highest ERI areas (i.e., those that promoted a high degree of pedestrian mobility) also tended to be the highest pSSD areas (i.e., those that had high fuel separation). Indeed, these areas likely represent ideal safety zones, given their provision of SSD and ease of movement within. ERI and VI were the least correlated among the three metrics (r = 0.13). As with pSSD, areas that had high ERI (>0.6) were most likely to also feature high VI – these are likely the same safety zone-suitable areas just discussed. However, there are many areas that have relatively high VI with relatively low ERI and relatively low VI with relatively high ERI. With respect to the former cases, these could be cliffs, steep mountain peaks and ridges, where foot travel is limited, but visibility is generally high. With respect to the latter cases, there are many vegetation types within this study area where visibility is low, due to the presence of tall trees, but mobility is high, due to the sparseness of understory vegetation. One example of this is ponderosa pine forests, which are abundant throughout this study area and feature tall canopies but often feature open, grassy understory areas that are easily traversed on foot. Taken together, the fact that these metrics are at least somewhat correlated points towards opportunities for identification of areas that are generally better or worse for promoting firefighter safety. Simultaneously, the variance left unexplained in these correlations speaks to the individual value each metric provides.

An examination of the dominant vegetation types provided valuable insight into the spatial distribution of the GeoLCES metrics (Figure 11). Separate analyses of variance aimed at modeling each of the three GeoLCES metrics as a function of vegetation type revealed that 20% of variance in ERI, 45% of variance in VI, and 33% of variance in pSSD could be explained by vegetation type alone. We attribute ERI being the least explainable by vegetation type to the inherent variability in terrain and vegetation density within vegetation types. For example, a dense piñon-juniper woodland and a sparse piñon-juniper woodland, although mapped as belonging to the same vegetation type based on species dominance, will feature significantly different mobility levels. By comparison, vegetation type was able to account for a higher proportion of variance in VI and pSSD. Especially with respect to pSSD, there were only a few vegetation types that featured relatively high pSSD, all of which were grassland, shrubland, or non-vegetated. All of the tree-dominated vegetation types had near-zero pSSD values, given the fact that they are dominantly considered heat sources in our study, rather than potential safety zones.

VI had similar relationships to vegetation type as pSSD, with a few exceptions. Whereas pSSD was near zero in Madrean Encinal, Mogollon chaparral, and Rocky Mountain Gambel oak-mixed montane shrubland, VI had somewhat higher values in these vegetation types. All three of them feature mixtures of grasses, shrubs, and short-stature woodland trees, whose height may have been tall enough to necessitate a moderate fuel separation (low pSSD), but perhaps short enough to retain a useful degree of visibility over the top of the canopy. Southern Rocky Mountain ponderosa pine woodland, despite yielding low VI and pSSD, was the highest-mobility forest or woodland type. These forests can have tall trees, both making them inadequate for safety zones and impeding visibility, but they also have open understories, facilitating efficient pedestrian travel. Conversely, North American warm desert bedrock cliff and outcrop tended to have somewhat higher VI, given the lack of vegetation and potential for providing localized high points with large viewsheds, but lower ERI, given the terrain roughness that they feature.

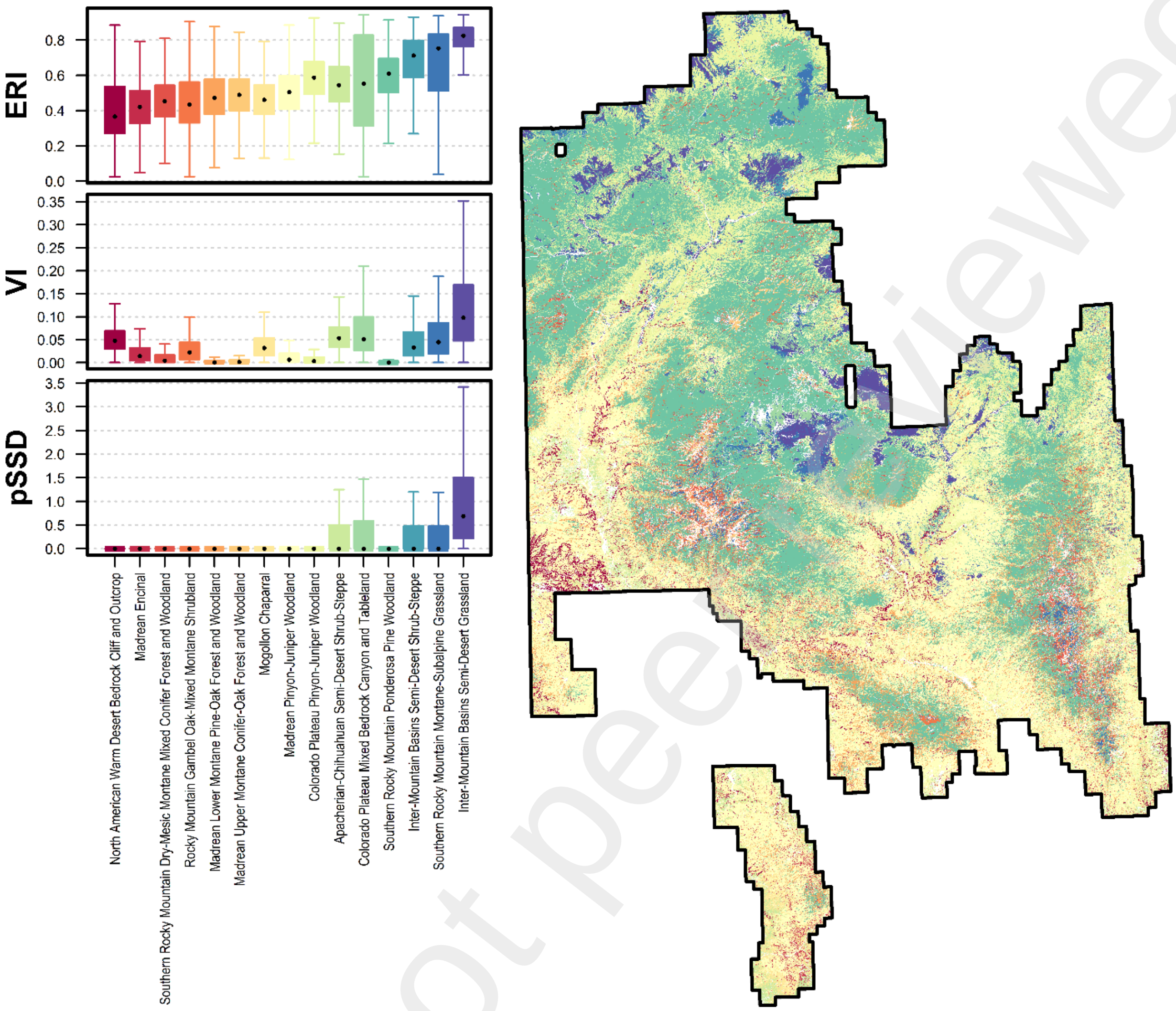

Figure 11. *Comparison between the three GeoLCES metrics and 2020 LANDFIRE Existing Vegetation Type data. The three boxplots on the left represent the distribution of GeoLCES pixel values grouped by the 15 most abundant vegetation types throughout the study area. Taken together, these vegetation types comprise 95% of the study area. The colors of the vegetation types in the box plots correspond to the colors on the map, ordered by the average GeoLCES metric values from lowest (left, red) to highest (right, purple).*

The results of our use-case demonstration can be seen in Figure 12 and Table 4. Taken together, the 51.7km^2 Doagy Fire was encompassed by nearly 36km of containment line (Division A: 14km; Division W: 11km; Division F: 11km). The average ERI along the containment line was 0.689 suggesting that, on average, one could evacuate with nearly 70% of optimal speed from positions along the containment line based on vegetation present before the line was established. The average VI was 0.084, meaning only 8.4% of one's surroundings could be seen within a 1km radius, on average, along and immediately surrounding the containment line. Thus, while mobility may have been generally high, visibility was generally low. This is likely attributable to the piñon-juniper woodland vegetation, dominant throughout the fire area, where relatively widely spaced trees can promote efficient walking but low (2-5m) and dense canopies can limit local-scale visibility. There were two areas that had potentially viable safety zones, one in the northwest and one in the northeast, which were desert grassland-dominated, relatively flat areas.

Breaking the results down by division, Division W had the best safety zone access and highest mobility, though the middle third of the containment line (~4-8km) featured limited visibility. If Division W hand crews were to be sent to this middle section of the containment line, it would be critical to have a well-placed lookout providing them with visibility support. Division A was farthest, on average, from a safety zone, with portions of the line being over 6km from the nearest safety zone, though it is worth noting that firefighters often use already-burned ("black") areas as safety zones, which would not be accounted for in these pre-fire data. Division A also had the lowest average visibility, possibly giving this division the highest hazard potential of the three. This is especially true towards the end of their containment line, where ERI was low, VI was generally less than 5%, and distance to safety zone was at a maximum. Armed with this information, a Division Supervisor might focus attention on whether Division A had sufficient safety zone access. Division F featured the highest average visibility, the lowest mobility, and a middling distance to the nearest safety zone. Much of Division F's containment line fell within a narrow valley, which at once provides a good view of surrounding valley walls and mountains, but limits mobility. It had good access to a safety zone on the far end of its containment line, but the beginning of the line was over 5km from the nearest safety zone. However, although not shown in Figure 12, there was an area less than 1km from the Division F containment line that featured a pSSD of 0.86, meaning it provided 86% of SSD – nearly suitable for a safety zone. With mechanical or fire-induced manipulation of the fuels, that area could potentially have been modified to meet suitability requirements.

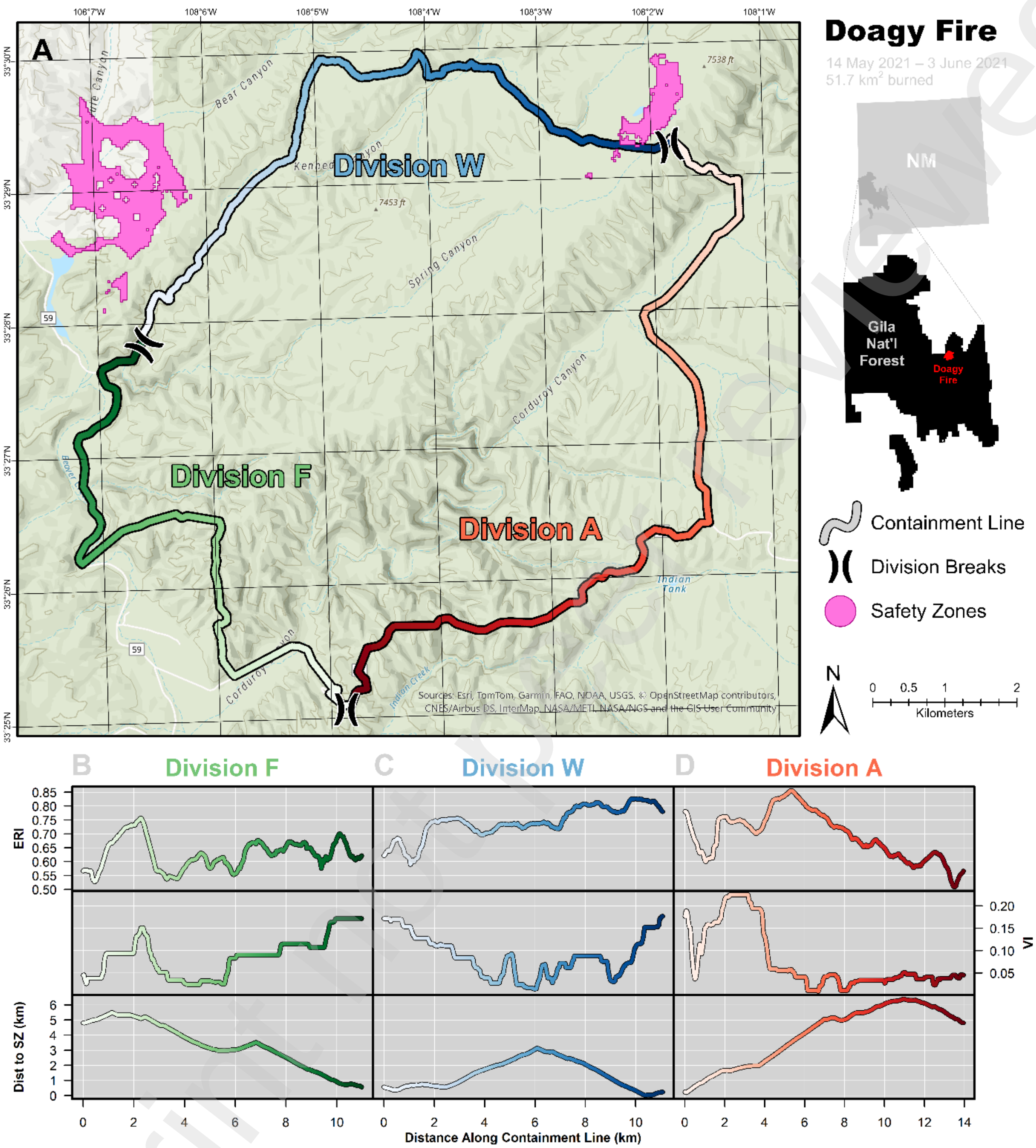

Figure 12. Operational use-case demonstration of GeoLCES. (A) A map of the containment line, split into three divisions, surrounding the 2021 Doagy Fire that occurred within our study area. The map also shows potential safety zones, mapped as areas with pSSD ≥ 1. (B-D) Graphs that quantify ERI (top), VI (middle), and distance to the nearest safety zone (bottom) for each of the three division's containment lines. The color of the lines in (B-D) correspond to the color of the lines in (A), with all representing distance along the lines, to facilitate direct visual comparison.

Table 4. Mean ERI, VI, and distance to the nearest safety zone (SZ) along each of the three divisions' sections of the containment line, as well as the containment line as a whole.

Division	Mean ERI	Mean VI	Mean Distance to SZ (km)
A	0.695	0.078	4.020

F	0.628	0.088	3.321
W	0.743	0.087	1.409
All	**0.689**	**0.084**	**3.005**

4. Discussion

One of the most important decisions made by wildland fire incident managers is where to direct resources to best provide a safe and effective response. Indeed, “safe and effective response” was defined as the highest priority in the US National Cohesive Wildland Fire Management Strategy. With respect to the effectiveness component, firefighters must be placed strategically on the landscape so as to minimize fire spread towards homes, communities, and other values at risk. There are many datasets available to incident management personnel to help maximize fire response effectiveness, including potential operational delineations [58], suppression difficulty index [59,60], and potential control locations [61]. These datasets are among those provided by operational decision support tools such as the Wildland Fire Decision Support System (WFDSS) and the Risk Management Assistance (RMA) dashboard, and are widely used in the US fire management community to increase response effectiveness [62–64]. Although given equal or sometimes greater weight than effectiveness, the safety component of “safe and effective response” has fewer operational datasets to facilitate robust, spatially explicit evaluation of wildland firefighter safety. The Wildland Firefighter Estimated Ground Evacuation Time and Snag Hazard are two examples of widely used, safety-focused datasets, but are somewhat narrow in their scope, with the former being focused on travel time to hospitals and the latter focused on the likelihood of snag fall [65–67]. In this study, we have introduced GeoLCES: a new, multivariate set of spatial metrics designed to be analyzed in concert with one another to facilitate the pre-fire evaluation and implementation of one of the most important safety protocols employed by wildland firefighters.

GeoLCES’s reliance on lidar is both a strength and a potential weakness. The strength lies in lidar’s unparalleled ability to map terrain and vegetation structure in a manner and with a resolution that is most pertinent to assessing firefighter safety. For example, ERI is heavily influenced by ground surface roughness, which is a measure only reliably attainable through the generation of a very high-resolution DTM. ERI also depends on vegetation density near the ground surface – another metric where lidar’s mapping capacity vastly exceeds that of other datasets. VI is derived from viewsheds, which are immensely more accurate and precise when based on high-resolution, lidar-derived DSMs. Similarly, pSSD is most strongly influenced by vegetation height, for which lidar is the gold standard data source of broad-scale measurement. The strengths of lidar in deriving incomparably accurate proxies for firefighter safety are clear. However, lidar – especially airborne lidar – is not available everywhere. Thanks to the USGS 3D Elevation Program, most of the contiguous US now has lidar data, but given the vegetation structural changes that occur in fire-prone portions of the country, much of the data – at least the portions of the data used for measuring vegetation structure – can quickly become outdated. Indeed, several major fires have even occurred within our study area in the time since the lidar data we used were flown, rendering our GeoLCES metrics inaccurate within recent fire extents.

Although we used Gila National Forest as a case study, the primary objective of this study was not to map a static product that could be used in perpetuity. It was to introduce an analytical framework, describe it in sufficient methodological detail to facilitate replication, discuss the potential management implications of applying the framework, demonstrate its application on an operationally useful scale (i.e., a US National Forest), and provide a specific, operationally relevant use case example. Thus, the fact that fires have altered fuel structure since our study's lidar data were flown does not substantively affect the work we have presented here. We designed GeoLCES to be broadly applicable and agnostic to a specific study area. All that is required for input is a lidar point cloud – be it one that is already in existence or one that could be specifically collected in a targeted manner at the scale of an individual incident to facilitate pre-fire decision support. The recent proliferation of lidar-equipped unoccupied aerial systems could be employed with minimal effort to map GeoLCES at a more local scale where there are no existing lidar data or those data are out of date.

In the complete absence of lidar data, it is possible that alternative, more widely available datasets could be used as substitutes. Our analyses of variance that compared GeoLCES metrics to LANDFIRE data clearly showed that vegetation type alone was able to explain a potentially useful amount of variance in at least VI, and to a lesser extent pSSD and ERI. Many of the metrics GeoLCES relies on (e.g., vegetation height, elevation, slope) are available on a US-wide or even global basis; however, they are produced at much coarser resolutions than that which GeoLCES currently relies on. Future work should seek to quantify the accuracy and management implication tradeoffs between GeoLCES versions produced with differing input datasets that vary in precision and spatiotemporal availability.

Each element of GeoLCES possesses its own uncertainty. VI, as mapped by VisiMod, is a modeled product, and thus has inherent error. Our demonstration of mapping VI in Gila National Forest yielded high predictive performance (Figure 6). However, individual pixel-level errors still persisted. We also utilized an omnidirectional VI to capture general situational awareness. In fighting fire, visibility in the direction of the fire may be of higher importance. Directional visibility can be modeled using VisiMod based on a given range of view angles [34]. Although we believe STRIDE represents the best-available and most relevant travel rate prediction model for assessing mobility in diverse environments, STRIDE was not developed with data from wildland firefighters. Given the above-average fitness and experience traversing complex landscapes on foot, firefighters likely move faster than the average individual. However, ERI being a proportional measure of mobility rather than an absolute measure of speed likely minimizes the effect of this limitation. pSSD is driven by the best-available fire physics and in situ measurements, but quantifying the spatial dimensions of heat exposure is constantly evolving as more data become available. The SSD calculation in Eq. 2 and the multiplicative factors in Table 2 are useful guidelines that err on the side of caution, but they may still change over time as the science evolves. Furthermore, it is common for firefighters to leverage areas that have already burned ("black") as safety zones, which would not be accounted for in this pre-fire decision support dataset.

In light of these uncertainties, it is critically important to mention the fact that GeoLCES, like all other spatial decision support datasets, should not be accepted at face value without field validation. We do not propose GeoLCES as a replacement for the experience and intuition that firefighters bring to their own *in situ* safety evaluation. Instead, we propose it as a supplement thereto, aimed at increasing the efficiency, consistency, and reliability of their safety protocol implementation. But every element of GeoLCES has inherent uncertainty, from the travel rate equation that drives ERI to the modeled visibility outputs from *VisiMod* to the potential landscape structural changes that occurred since lidar data were collected. Thus, GeoLCES should be treated as a useful pre-fire decision support tool to inform safety, and not an absolute measure of safety.

5. Conclusions

Wildland firefighters put their lives on the line to help minimize the harmful effects of fire. Over the past decade, the role of spatial data in decision support has expanded, our understanding of the mechanisms that drive firefighter safety have improved, and the availability of invaluable and highly safety-relevant datasets such as airborne lidar has grown exponentially. During this same time frame, we have worked to develop several spatial metrics that address individual components of firefighter safety, including ERI, VI, and pSSD. Though potentially valuable on their own, only through their combined, simultaneous evaluation can a more comprehensive understanding of firefighter safety be obtained. LCES is among the most important safety protocols available to wildland firefighters, yet its implementation is, to date, driven entirely by *in situ* information. Though ground-level, incident-specific, locally informed knowledge plays and should continue to play a critical role in LCES, we believe that leveraging the best-available data, science, and computational algorithms can make LCES safer and more effective. GeoLCES offers a new analytical framework that, if properly applied, has the potential to increase wildland firefighter safety. In an era of increasing wildfire activity, we can and should leverage all of the best tools available to mitigate risk to a population of professionals who engage in critical, life-saving work.

We recognize that there are already a host of extant, operational spatial decision support datasets and tools. Continually throwing new information at an already information-rich problem has the potential to exceed firefighters' capacity to ingest that new information and yield actionable fire management strategies. Thus, it is important that we be judicious in the introduction of new tools into the wildland fire community and work closely with fire personnel everywhere along the chain of command to ensure that our technological advances are meeting the needs of the end user community. Here we have introduced GeoLCES to the scientific and fire management communities as an important first step in that process.

Author Contributions: CRediT

Michael Campbell: Conceptualization, Methodology, Software, Validation, Formal Analysis, Investigation, Data Curation, Writing – Original Draft, Writing – Review & Editing, Visualization, Supervision, Project Administration, Funding Acquisition; **Katherine Mistick:** Methodology, Software, Formal Analysis, Data Curation, Writing – Review & Editing; **Daniel Jimenez:** Conceptualization, Writing – Review & Editing, Supervision, Funding Acquisition; **Philip Dennison:** Conceptualization, Methodology, Resources, Writing – Review & Editing, Supervision, Project Administration, Funding Acquisition.

Funding Sources

This work was funded by the USDA Forest Service [grant numbers 24-CR-11221637-165 & 21-CS-11221636-120] and the National Science Foundation [grant number 2117865].

References

[1] P. Withen, Climate Change and Wildland Firefighter Health and Safety, New Solut 24 (2015) 577–584. https://doi.org/10.2190/NS.24.4.i.

[2] J.D. Cohen, Reducing the wildland fire threat to homes: Where and how much?, In: Gonzales-Caban, Armando; Omi, Philip N., Technical Coordinators. Proceedings of the Symposium on Fire Economics, Planning, and Policy: Bottom Lines; 1999 April 5-9. San Diego, CA. Gen. Tech. Rep. PSW-GTR-173. Albany, CA: U.S. Department of Agriculture, Forest Service, Pacific Southwest Research Station. p. 189-195 (1999). https://research.fs.usda.gov/treesearch/5603 (accessed March 5, 2025).

[3] K. Navarro, Working in Smoke: Wildfire Impacts on the Health of Firefighters and Outdoor Workers and Mitigation Strategies, Clin Chest Med 41 (2020) 763–769. https://doi.org/10.1016/j.ccm.2020.08.017.
[4] T. Schoennagel, J.K. Balch, H. Brenkert-Smith, P.E. Dennison, B.J. Harvey, M.A. Krawchuk, N. Mietkiewicz, P. Morgan, M.A. Moritz, R. Rasker, M.G. Turner, C. Whitlock, Adapt to more wildfire in western North American forests as climate changes, Proceedings of the National Academy of Sciences 114 (2017) 4582–4590. https://doi.org/10.1073/pnas.1617464114.
[5] C. Eriksen, Coexisting with wildfire: strengthening collective capacity by changing the status quo, Fire Ecology 20 (2024) 59. https://doi.org/10.1186/s42408-024-00290-y.
[6] M.B. Held, M.R. Ragland, S. Wood, A. Pearson, S.W. Pearson, O. Chenevert, R.M. Granberg, R.M. Verble, Environmental health of wildland firefighters: a scoping review, Fire Ecology 20 (2024) 16. https://doi.org/10.1186/s42408-023-00235-x.
[7] C. Butler, S. Marsh, J.W. Domitrovich, J. Helmkamp, Wildland firefighter deaths in the United States: A comparison of existing surveillance systems, J Occup Environ Hyg 14 (2017) 258–270. https://doi.org/10.1080/15459624.2016.1250004.
[8] P. Gleason, Lookouts, Communications, Escape Routes, and Safety Zones, Wildland Fire Leadership (1991). https://www.fireleadership.gov/toolbox/documents/lces_gleason.html (accessed February 17, 2017).
[9] K.A. Mistick, M.J. Campbell, P.E. Dennison, Visibility-informed mapping of potential firefighter lookout locations using maximum entropy modelling, Int. J. Wildland Fire 33 (2024). https://doi.org/10.1071/WF24065.
[10] J. Steele, Effective firefighter safety zone size: a perception of firefighter safety, 4th International Wildland Fire Safety Summit (2000) 10–12.
[11] M.J. Campbell, P.E. Dennison, M.P. Thompson, B.W. Butler, Assessing Potential Safety Zone Suitability Using a New Online Mapping Tool, Fire 5 (2022) 5. https://doi.org/10.3390/fire5010005.
[12] M.J. Campbell, P.E. Dennison, B.W. Butler, A LiDAR-based analysis of the effects of slope, vegetation density, and ground surface roughness on travel rates for wildland firefighter escape route mapping, Int. J. Wildland Fire 26 (2017) 884–895. https://doi.org/10.1071/WF17031.
[13] J. Gajardo, M. García, D. Riaño, Applications of Airborne Laser Scanning in Forest Fuel Assessment and Fire Prevention, in: M. Maltamo, E. Næsset, J. Vauhkonen (Eds.), Forestry Applications of Airborne Laser Scanning: Concepts and Case Studies, Springer Netherlands, Dordrecht, 2014: pp. 439–462. https://doi.org/10.1007/978-94-017-8663-8_22.
[14] P.E. Dennison, G.K. Fryer, T.J. Cova, Identification of firefighter safety zones using lidar, Environmental Modelling & Software 59 (2014) 91–97. https://doi.org/10.1016/j.envsoft.2014.05.017.
[15] K.A. Mistick, P.E. Dennison, M.J. Campbell, M.P. Thompson, Using Geographic Information to Analyze Wildland Firefighter Situational Awareness: Impacts of Spatial Resolution on Visibility Assessment, Fire 5 (2022) 151. https://doi.org/10.3390/fire5050151.
[16] E. Gabor, Words matter: radio misunderstandings in wildland firefighting, Int. J. Wildland Fire 24 (2015) 580–588. https://doi.org/10.1071/WF13120.
[17] J. Baek, Y. Choi, Comparison of Communication Viewsheds Derived from High-Resolution Digital Surface Models Using Line-of-Sight, 2D Fresnel Zone, and 3D Fresnel Zone Analysis, ISPRS International Journal of Geo-Information 7 (2018) 322. https://doi.org/10.3390/ijgi7080322.
[18] N.C. Inglis, J. Vukomanovic, J. Costanza, K.K. Singh, From viewsheds to viewscapes: Trends in landscape visibility and visual quality research, Landscape and Urban Planning 224 (2022) 104424. https://doi.org/10.1016/j.landurbplan.2022.104424.
[19] G.K. Fryer, P.E. Dennison, T.J. Cova, Wildland firefighter entrapment avoidance: modelling evacuation triggers, Int. J. Wildland Fire 22 (2013) 883–893. https://doi.org/10.1071/WF12160.

[20] J. Sheng, X. Li, X. Wang, Y. Wang, S. Li, D. Li, S. Sun, L. Zhao, An escape route planning model based on wildfire prediction information and travel rate of firefighters, Int. J. Wildland Fire 33 (2024). https://doi.org/10.1071/WF23166.
[21] W. Jiang, J. Zhou, J. Zhu, G. Su, F. Wang, FRI: A firefighter risk index using spatiotemporal modelling of wildfire spread and individual travel, International Journal of Disaster Risk Reduction 117 (2025) 105151. https://doi.org/10.1016/j.ijdrr.2024.105151.
[22] B.W. Butler, J.D. Cohen, Firefighter Safety Zones: A Theoretical Model Based on Radiative Heating, Int. J. Wildland Fire 8 (1998) 73–77. https://doi.org/10.1071/wf9980073.
[23] B.W. Butler, Wildland firefighter safety zones: a review of past science and summary of future needs, Int. J. Wildland Fire 23 (2014) 295–308. https://doi.org/10.1071/WF13021.
[24] L. Zárate, J. Arnaldos, J. Casal, Establishing safety distances for wildland fires, Fire Safety Journal 43 (2008) 565–575. https://doi.org/10.1016/j.firesaf.2008.01.001.
[25] W.G. Page, B.W. Butler, An empirically based approach to defining wildland firefighter safety and survival zone separation distances, International Journal of Wildland Fire 26 (2017) 655–667.
[26] J. Fayad, G. Accary, F. Morandini, F.-J. Chatelon, L. Rossi, T. Marcelli, D. Cancellieri, V. Cancellieri, Y. Rahib, D. Morvan, S. Meradji, A. Pieri, J.-Y. Duret, J.-L. Rossi, Numerical Assessment of Safe Separation Distance in the Wildland–Urban Interfaces, Fire 6 (2023) 209. https://doi.org/10.3390/fire6050209.
[27] W.R. Franklin, C. Ray, Higher isn't necessarily better: Visibility algorithms and experiments, in: Advances in GIS Research: Sixth International Symposium on Spatial Data Handling, Taylor & Francis Edinburgh, 1994: pp. 751–770.
[28] M.J. Campbell, W.G. Page, P.E. Dennison, B.W. Butler, Escape Route Index: A Spatially-Explicit Measure of Wildland Firefighter Egress Capacity, Fire 2 (2019) 40. https://doi.org/10.3390/fire2030040.
[29] J. Shan, C.K. Toth, Topographic Laser Ranging and Scanning: Principles and Processing, Second Edition, CRC Press, 2018.
[30] J.R. Parent, Q. Lei-Parent, Rapid viewshed analyses: A case study with visibilities limited by trees and buildings, Applied Geography 154 (2023) 102942. https://doi.org/10.1016/j.apgeog.2023.102942.
[31] M.L. Miller, Analysis of Viewshed Accuracy with Variable Resolution LIDAR Digital Surface Models and Photogrammetrically-Derived Digital Elevation Models, Virginia Tech, 2011. http://hdl.handle.net/10919/35692 (accessed March 6, 2025).
[32] P.F. Fisher, Algorithm and implementation uncertainty in viewshed analysis, International Journal of Geographical Information Systems 7 (1993) 331–347. https://doi.org/10.1080/02693799308901965.
[33] B. Kaučič, B. Zalik, Comparison of viewshed algorithms on regular spaced points, in: Proceedings of the 18th Spring Conference on Computer Graphics, Association for Computing Machinery, New York, NY, USA, 2002: pp. 177–183. https://doi.org/10.1145/584458.584487.
[34] K.A. Mistick, M.J. Campbell, VisiMod: Map Modeled Visibility Index Across Wildland Landscapes, (2023). https://github.com/kamistick/VisiMod (accessed March 6, 2025).
[35] K.A. Mistick, M.J. Campbell, M.P. Thompson, P.E. Dennison, Using airborne lidar and machine learning to predict visibility across diverse vegetation and terrain conditions, International Journal of Geographical Information Science 37 (2023) 1728–1764. https://doi.org/10.1080/13658816.2023.2224421.
[36] I. Herzog, Theory and practice of cost functions, in: Fusion of Cultures. Proceedings of the 38th Annual Conference on Computer Applications and Quantitative Methods in Archaeology, Granada, Spain, 2010: pp. 375–382.

[37] D.A. White, The Basics of Least Cost Analysis for Archaeological Applications, Advances in Archaeological Practice 3 (2015) 407–414. https://doi.org/10.7183/2326-3768.3.4.407.

[38] W. Tobler, Three presentations on geographical analysis and modeling, National Center for Geographic Information and Analysis, University of California at Santa Barbara, 1993.

[39] M.E. Alexander, G.J. Baxter, G.R. Dakin, Travel rates of Alberta wildland firefighters using escape routes, in: B.W. Butler, M.E. Alexander (Eds.), Human Factors - 10 Years Later, International Association of Wildland Fire, Missoula, MT, 2005. http://citeseerx.ist.psu.edu/viewdoc/download?doi=10.1.1.535.9337&rep=rep1&type=pdf (accessed February 23, 2017).

[40] P.W. Richmond, A.W. Potter, W.R. Santee, Terrain Factors for Predicting Walking and Load Carriage Energy Costs: Review and Refinement, Journal of Sport and Human Performance 3 (2015). https://doi.org/10.12922/jshp.v3i3.67.

[41] M.J. Campbell, S.L. Cutler, P.E. Dennison, A singular, broadly-applicable model for estimating on- and off-path walking travel rates using airborne lidar data, Sci Rep 14 (2024) 21393. https://doi.org/10.1038/s41598-024-71359-6.

[42] K.M. Brubaker, W.L. Myers, P.J. Drohan, D.A. Miller, E.W. Boyer, The Use of LiDAR Terrain Data in Characterizing Surface Roughness and Microtopography, Applied and Environmental Soil Science 2013 (2013) e891534. https://doi.org/10.1155/2013/891534.

[43] D. Frankman, B.W. Webb, B.W. Butler, D. Jimenez, J.M. Forthofer, P. Sopko, K.S. Shannon, J.K. Hiers, R.D. Ottmar, D. Frankman, B.W. Webb, B.W. Butler, D. Jimenez, J.M. Forthofer, P. Sopko, K.S. Shannon, J.K. Hiers, R.D. Ottmar, Measurements of convective and radiative heating in wildland fires, Int. J. Wildland Fire 22 (2012) 157–167. https://doi.org/10.1071/WF11097.

[44] J.R. Gallacher, B. Ripa, B.W. Butler, T.H. Fletcher, Lab-scale observations of flame attachment on slopes with implications for firefighter safety zones, Fire Safety Journal 96 (2018) 93–104. https://doi.org/10.1016/j.firesaf.2018.01.002.

[45] B. Butler, S. Quarles, C. Standohar-Alfano, M. Morrison, D. Jimenez, P. Sopko, C. Wold, L. Bradshaw, L. Atwood, J. Landon, J. O'Brien, B. Hornsby, N. Wagenbrenner, W. Page, Exploring fire response to high wind speeds: fire rate of spread, energy release and flame residence time from fires burned in pine needle beds under winds up to 27 m s−1, Int. J. Wildland Fire 29 (2019) 81–92. https://doi.org/10.1071/WF18216.

[46] National Wildfire Coordinating Group, NWCG Guide to Fire Behavior Assessment, 2024. https://www.nwcg.gov/publications/pms437-1 (accessed April 22, 2025).

[47] W.A. Bechtold, P.L. Patterson, eds., The Enhanced Forest Inventory and Analysis Program--national Sampling Design and Estimation Procedures, USDA Forest Service, Southern Research Station, 2005.

[48] G.I. Snyder, The 3D Elevation Program: summary of program direction, U.S. Geological Survey, Reston, VA, 2012. http://pubs.er.usgs.gov/publication/fs20123089.

[49] J.-R. Roussel, D.A. (Reviews the documentation), F.D.B. (Fixed bugs and improved catalog features), A.S.M. (Implemented wing2015() for segment_snags()), B.J.-F. (Contributed to R. for track_sensor()), G.D. (Implemented G. for track_sensor()), lidR: Airborne LiDAR Data Manipulation and Visualization for Forestry Applications, (2020). https://CRAN.R-project.org/package=lidR (accessed October 8, 2020).

[50] R Core Team, R: A language and environment for statistical computing., (2021). https://www.R-project.org/.

[51] U.S. Geological Survey, National Hydrography Dataset Plus High Resolution (NHDPlus HR), (2023). https://www.sciencebase.gov/catalog/item/57645ff2e4b07657d19ba8e8 (accessed February 13, 2024).

[52] Microsoft, US Building Footprints, (2024). https://github.com/microsoft/USBuildingFootprints (accessed February 13, 2024).
[53] M.N. Wright, A. Ziegler, ranger: A Fast Implementation of Random Forests for High Dimensional Data in C++ and R, J. Stat. Soft. 77 (2017). https://doi.org/10.18637/jss.v077.i01.
[54] P. Probst, M.N. Wright, A.-L. Boulesteix, Hyperparameters and tuning strategies for random forest, WIREs Data Mining and Knowledge Discovery 9 (2019) e1301. https://doi.org/10.1002/widm.1301.
[55] R.J. Hijmans, R. Bivand, E. Pebesma, M.D. Sumner, terra: Spatial Data Analysis, (2023). https://CRAN.R-project.org/package=terra (accessed January 22, 2023).
[56] J. van Etten, K. de Sousa, gdistance: Distances and Routes on Geographical Grids, (2020). https://CRAN.R-project.org/package=gdistance (accessed March 1, 2022).
[57] LANDFIRE, LANDFIRE Existing Vegetation Type, v2.2.0, (2020). https://landfire.gov/evt.php (accessed October 19, 2022).
[58] M.P. Thompson, C.D. O'Connor, B.M. Gannon, M.D. Caggiano, C.J. Dunn, C.A. Schultz, D.E. Calkin, B. Pietruszka, S.M. Greiner, R. Stratton, J.T. Morisette, Potential operational delineations: new horizons for proactive, risk-informed strategic land and fire management, Fire Ecol 18 (2022) 17. https://doi.org/10.1186/s42408-022-00139-2.
[59] F.R. y Silva, J.R.M. Martínez, A. González-Cabán, A methodology for determining operational priorities for prevention and suppression of wildland fires, Int. J. Wildland Fire 23 (2014) 544–554. https://doi.org/10.1071/WF13063.
[60] F.R.Y. Silva, C.D. O'Connor, M.P. Thompson, J.R.M. Martínez, D.E. Calkin, Modelling suppression difficulty: current and future applications, International Journal of Wildland Fire 29 (2020) 739–751. https://doi.org/10.1071/WF19042.
[61] C.D. O'Connor, D.E. Calkin, M.P. Thompson, An empirical machine learning method for predicting potential fire control locations for pre-fire planning and operational fire management, Int. J. Wildland Fire 26 (2017) 587–597. https://doi.org/10.1071/WF16135.
[62] M.P. Thompson, Decision making under uncertainty: Recommendations for the Wildland Fire Decision Support System (WFDSS), In: Keane, Robert E.; Jolly, Matt; Parsons, Russell; Riley, Karin. Proceedings of the Large Wildland Fires Conference; May 19-23, 2014; Missoula, MT. Proc. RMRS-P-73. Fort Collins, CO: U.S. Department of Agriculture, Forest Service, Rocky Mountain Research Station. p. 317-319. 73 (2015) 317–319.
[63] D.E. Calkin, C.D. O'Connor, M.P. Thompson, R. Stratton, Strategic Wildfire Response Decision Support and the Risk Management Assistance Program, Forests 12 (2021) 1407. https://doi.org/10.3390/f12101407.
[64] T.A. Beeton, M.D. Caggiano, M.M. Colavito, H. Ch'aska, Use of Risk Management Assistance During the 2021 Fire Season: A technical report, Southwest Ecological Restoration Institute, Fort Collins, CO, 2022. https://cfri.colostate.edu/wp-content/uploads/sites/22/2022/12/Beeton_RMA_USE_2021_WildfireSeason_Report.pdf (accessed May 31, 2024).
[65] C.J. Dunn, C.D. O'Connor, M.J. Reilly, D.E. Calkin, M.P. Thompson, Spatial and temporal assessment of responder exposure to snag hazards in post-fire environments, Forest Ecology and Management 441 (2019) 202–214. https://doi.org/10.1016/j.foreco.2019.03.035.
[66] K.L. Riley, C.D. O'Connor, C.J. Dunn, J.R. Haas, R.D. Stratton, B. Gannon, A National Map of Snag Hazard to Reduce Risk to Wildland Fire Responders, Forests 13 (2022) 1160. https://doi.org/10.3390/f13081160.
[67] M.J. Campbell, B.M. Gannon, O. Rahman, R.D. Stratton, P.E. Dennison, Wildland Firefighter Estimated Ground Evacuation Time Modeling to Support Risk-Informed Decision-Making, Fire 7 (2024) 292. https://doi.org/10.3390/fire7080292.

GeoLCES: Geospatial support for evaluating wildland firefighter lookouts, communications, escape routes, and safety zones

Michael J. Campbell[a,*], Katherine A. Mistick[a], Daniel M. Jimenez[b], Philip E. Dennison[a]

[a] School of Environment, Society & Sustainability, University of Utah, 260 South Central Campus Drive, Room 4625, Salt Lake City, UT, 84112
[b] Missoula Fire Sciences Laboratory, Rocky Mountain Research Station, USDA Forest Service, 5775 Highway 10 West, Missoula, MT, 59808

* Corresponding author: mickey.campbell@ess.utah.edu (email)